Correspondence to:
M. Berti,
matteo.berti@unibo.it

Physical Interpretation of Rainfall Thresholds for Runoff-Generated Debris Flows

Matteo Berti[1] [ID], **Martino Bernard[2]** [ID], **Carlo Gregoretti[2]** [ID], and **Alessandro Simoni[1]** [ID]

[1]Department of Biological, Geological and Environmental Sciences, University of Bologna, Bologna, Italy, [2]Department of Land Environment Agriculture and Forestry, University of Padua, Padua, Italy

Abstract Rainfall thresholds for the occurrence of debris flows are commonly defined by Intensity-Duration curves (*ID* thresholds). Interestingly, many empirical *ID* thresholds show up as straight lines in a log-log plot and therefore can be expressed by power-law functions of the form $I = \alpha \cdot D^{\beta}$, where α is the scaling coefficient and β is the exponent of the power function. The different values of α and β reflect the variability of geological and hydrological conditions in the different areas. In most cases, however, field conditions are so complex that a quantitative interpretation of the empirical rainfall threshold is impossible and the physical meaning of α and β remains obscure. In this work, we provide a physical interpretation of the rainfall thresholds that characterize an active debris flow catchment in the Eastern Italian Alps (the Dimai Basin, Belluno Province). The catchment is affected by frequent debris flows generated by surface-water runoff and has been monitored since 2010 to investigate the initiation process. Monitoring data allowed for the detection of two rainfall thresholds: a lower one that identifies the arrival of water in the initiation area (Catchment Outflow Threshold) and an upper one that identifies the initiation of debris flows by channel runoff (Debris Flow Threshold). We demonstrate that these two thresholds can be satisfactorily reproduced by a simple physically based model in which the excess rainfall is routed over the catchment using a kinematic-wave scheme. This simple analysis provides a sound explanation of the observed thresholds and can be used to develop physically based thresholds for runoff-generated debris flows.

1. Introduction

Debris flows are rapid, destructive landslides common in many mountainous areas (Cruden & Varnes, 1996; Hungr et al., 2001; Hutchinson, 1988). Because of their high velocity, long runout, and high impact forces, debris flows are one of the most dangerous geomorphic hazards in steep catchments (Iverson, 1997; Jakob & Hungr, 2005; Takahashi, 2019). Rainfall is the main triggering factor for debris flows, so most regional warning systems rely on the use of rainfall thresholds to predict debris flow occurrence (Abancó et al., 2016; Aleotti, 2004; Baum & Godt, 2010; Guo et al., 2013; Hürlimann et al., 2014; Osanai et al., 2010; Staley et al., 2017). These thresholds are usually empirically derived from the rainfall records that caused past debris flows in a certain area (Cannon et al., 2008; Chang et al., 2008; Huang et al., 2015; Giannecchini et al., 2012; Iadanza et al., 2016; Saito et al., 2010; Zhou & Tang, 2014). More than 200 rainfall thresholds were published in the last 40 years following this empirical approach (Guzzetti et al., 2007; Segoni et al., 2018) with the common goal of providing a practical tool for hazard mitigation.

The physical interpretation of empirical thresholds has been given less attention. In particular, the reason why most intensity-duration (*ID*) thresholds take the form of power-law functions $I = \alpha D^{-\beta}$ (where α is a scaling factor and β is a scaling exponent) is essentially unknown, as well as the physical meaning the parameters α and β. This dearth of knowledge is primarily due to the uncertainties associated with empirical thresholds. Even for specific regions, it is seldom possible to have reliable data on landslide occurrence, triggering rainfall, and all the physical factors that control slope stability. This poor understanding, together with the complexity that characterizes natural slopes in wide areas, usually prevents an adequate assessment of slope processes and a full understanding of the physical system (Chowdhury & Flentje, 2002; Corominas et al., 2014; Van Asch et al., 2007).

To address this limitation, several researchers explored the use of coupled hydrology and slope stability models to obtain physically based rainfall thresholds (Fusco et al., 2019; Peres & Cancelliere, 2014; Salciarini et al., 2012; Wu et al., 2015). Others combined slope stability models with pore water pressure measurements or soil moisture data collected in the field or estimated by satellite products (Kirschbaum et al., 2015; Posner & Georgakakos, 2015; Thomas et al., 2018). Quantitative prediction methods however suffer from substantial drawbacks such as the high degree of oversimplification, the need for a large amount of input data, and the uncertainty in model results that limit their usefulness in practical applications. As a matter of fact, empirical methods are still the only alternative to derive operational rainfall thresholds, although the physical meaning of these functions remains obscure.

In this study, we use simple hydrological concepts to explain the empirical rainfall threshold for debris flows triggering in a typical Alpine catchment (the Dimai Basin, Cortina d'Ampezzo, Italy). The catchment is affected by frequent debris flows generated by surface-water runoff and has been monitored since 2010 to investigate the initiation process. The initiation process of runoff-generated debris flows is different from that of landslide-induced debris flows. Debris flow mobilization from landslides occurs as a result of the mechanical failure of the soil, due to the buildup of positive pore pressure during intense rainfall events (Gabet & Mudd, 2006; Iverson, 1997, 2000; Montgomery et al., 2009). Instead, debris flows produced by channel runoff occur by a variety of processes (progressive bulking, mass failure of the channel bed, and firehose effect) in which surface water, rather than groundwater, is the key factor (Coe, Cannon, et al., 2008; Coe, Kinner, et al., 2008; Kean et al., 2013; Okano et al., 2012). Over the years, many studies have been conducted to assess the critical surface discharge for debris flow initiation (Gregoretti & Dalla Fontana, 2008; Pastorello et al., 2020; Prancevic et al., 2014; Tognacca et al., 2000) as well as to identify the critical rainfall conditions (Cannon et al., 2011; Staley et al., 2013). In 2005, we developed a simple hydrological model to predict the occurrence of surface runoff in the initiation area of an Alpine debris flow in response to rainfall of different duration and intensity (Berti & Simoni, 2005). The model successfully reproduced the observed hydrological behavior of a monitored catchment and provided a first conceptual framework to obtain physically based thresholds. Despite these efforts, the mechanics of the initiation of runoff-generated debris flows is still less understood compared to landslide-induced debris flows, and there are few direct observations of this process (Kean et al., 2013; Ma et al., 2018; Yu et al., 2014). In this study, we present long-term data that provide new insight into the process of debris flow initiation by surface runoff and allow the physical understanding of the empirical rainfall threshold.

2. Study Area

The Dimai catchment is located on the western slope of the Pomagagnon Massif (2,540 m a.s.l.) in the dolomitic region of the Eastern Italian Alps (Figure 1). The catchment is dominated by two major geological units. First, the Dolomia Principale Formation (Upper Trias), which consists of carbonate rocks almost completely dolomitized attaining a total thickness of 500–1,000 m (Bosellini et al., 2003). These rocks outcrop in the upper part of the basin and form the scenic rock cliffs that characterize the landscape of the area. The second major geological unit is composed of Quaternary deposits, mostly derived from periodic rockfall from cliff faces and past glacial activity. They consist of coarse, poorly sorted debris which blanket the slopes from the cliff to the valley floor. The slope angle of the talus slopes varies from 5° at the valley bottom to over 35° close to the cliff.

Table 1 summarizes the characteristics of the Dimai catchment. The fan has an approximate area of 65.000 m^2, and it is mostly covered by forest. It extends from the fan apex of 690 m before reaching the main river (Figure 1). The lobate shape, small size, and relatively high steepness clearly indicate that the fan was mainly constructed by debris flows processes. The feeder channel is ephemeral being typically dry. At present, it flows along the right side of the fan, but avulsions are common during large events. At the fan apex, the channel has a depth of about 5 m (flow area 80–90 m^2), and it is confined by bouldery lateral levees left by previous events. Erosion appears slight for the first 100 m, as in this reach, debris flows tend to form terraced deposits inside the channel. For the next 350 m, from about 1,450 to 1,600 m of elevation, the channel is deeply incised into the talus at an average slope angle of 30°. Here, erosion dominates over deposition, and the channel reaches its maximum depth of 10 m. The upper reach of the channel, from about 1,600 to 1,710 m of elevation, is very steep (30–35°) with narrow confinement. The head of the channel (Figure 2) is located at
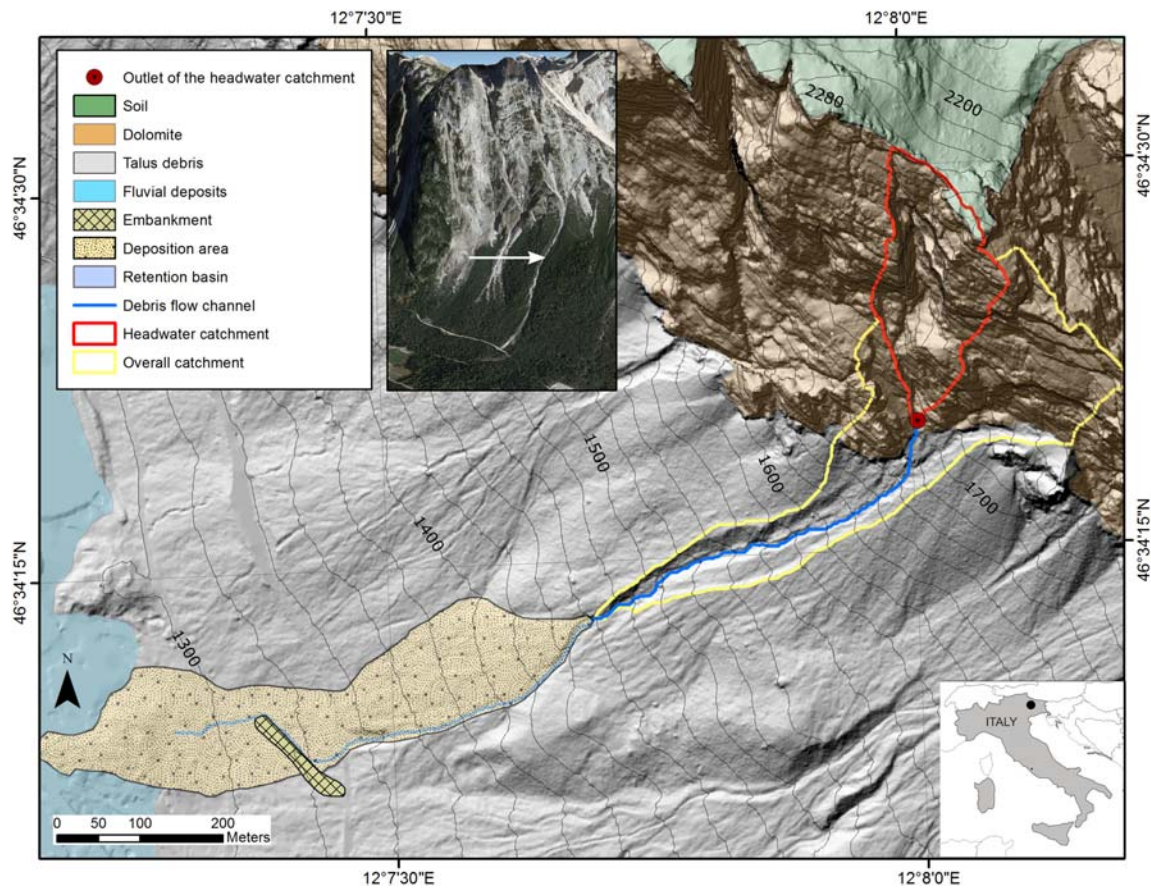
Figure 1. Geological map of the Dimai debris flow. The small inset shows a general view of the catchment (the white arrow indicates the Dimai debris flow channel). Elevation is in meter above sea level, contour interval 20 m.

the outlet of a small 30.000 m^2 of catchment characterized by extremely steep slopes with exposed bare rock (headwater catchment in Figure 1).

Debris flows are initiated just at the base of the rock cliff. The mobilization of the talus material is caused by a concentrated flow of water pouring off the headwater catchment. Intense rainfall generates overland flow on the rocky cliff, which is concentrated in steep bedrock channels and rapidly delivered at the outlet. Here, the water impacts the loose debris and starts to entrain the sediment from the bed and the channel banks. The process of sudden mobilization of debris at the exit of steep rock channels is known as "the firehose effect" (Coe, Cannon, et al., 2008; Coe, Kinner, et al., 2008; Godt & Coe, 2007; Johnson & Rodine, 1984; Larsen et al., 2006). The initial dilute flows become increasingly more laden as they propagate downstream. However, debris flows form very rapidly, and the first evidences of fully developed flows (such as internal levees or small deposition lobes within the channel) are generally found less than 100 m downstream the head of the channel. Critical conditions for debris flow triggering typically occur during the summer season (from June to September; Berti et al., 1999), when locally intense convective storms produce rainfall intensities sufficient to generate runoff in the channel. Both the catchment morphology and climatic conditions of Dimai are typical of the active debris flow basins in the Dolomites.

3. Materials and Methods

3.1. Monitoring System

A monitoring system was installed in July 2010 to investigate the hydrologic response to rainfall in the initiation area of the debris flow. Figure 3 shows the location and the architecture of the system. Rainfall is measured by a tipping-bucket rain gage (ARG100) with a standard sensitivity of 0.2 mm of rain per tip. The distance between the rain gage and the centroid of the headwater is about 150 m. Two video cameras

Table 1
Physical Characteristics of the Dimai Basin

Overall catchment (above the fan)	Area (m^2)	97,880
	Maximum elevation (m)	2,270
	Minimum elevation (m)	1,460
	Surface geology (percentage)	67% rock
		33% debris
Headwater catchment	Area (m^2)	30,440
	Maximum elevation (m)	2,270
	Minimum elevation (m)	1,710
	Mean slope (°)	63°
	Surface geology (percentage)	almost 100% rock
Channel (above the fan)	Length (m)	450
	Mean slope (°)	30
	Maximum depth (m)	10
	Maximum width (m)	35
Fan	Area (m^2)	70,060
	Elevation of apex (m)	1,460
	Relief (m)	170
	Length (m)	690
	Mean slope (°)	16
	Melton's ruggedness number	0.64

capture the response of the basin to precipitation inputs: cam1 looks upstream to the catchment outlet; cam2 looks downstream into the debris flow channel (Figure 3r). Each camera has a 256-GB hard drive that can record up to 70-hr video file at a resolution of 1,024 × 768 and 10 fps.

A sharp-crested weir measures the discharge at the outlet of the headwater catchment (Figures 4a and 4b). Building the weir took considerable effort. The rock behind the weir was excavated to create an approximately rectangular basin (1.8 m wide and 2.0 m long), then the walls were sealed with concrete and part of the upstream channel stabilized with gabions to reduce bedload transport. A pressure sensor was finally mounted into a plastic pipe fixed at the bottom of the basin to measure the water level. The sensor is a temperature-compensated piezoresistive transducer mounted in a stainless steel housing (Keller series 26 W). The full-scale range is 0.5 bar, and the accuracy is 1 mm of water. The weir required frequent
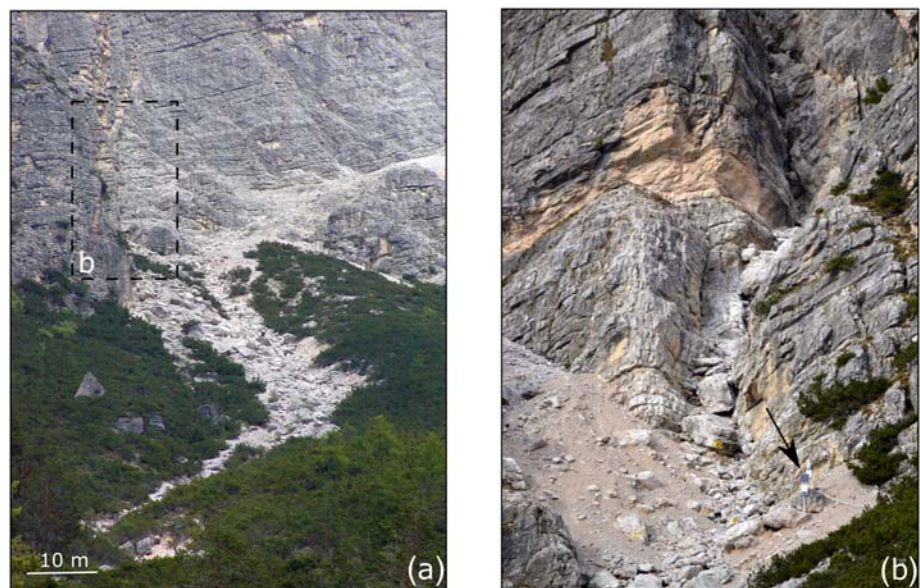

Figure 2. Pictures showing the initiation area of the debris flow: (a) general view of the upper reach of the channel below the dolomite cliff; (b) close view of the outlet of the headwater catchment; the arrow indicates the monitoring station.
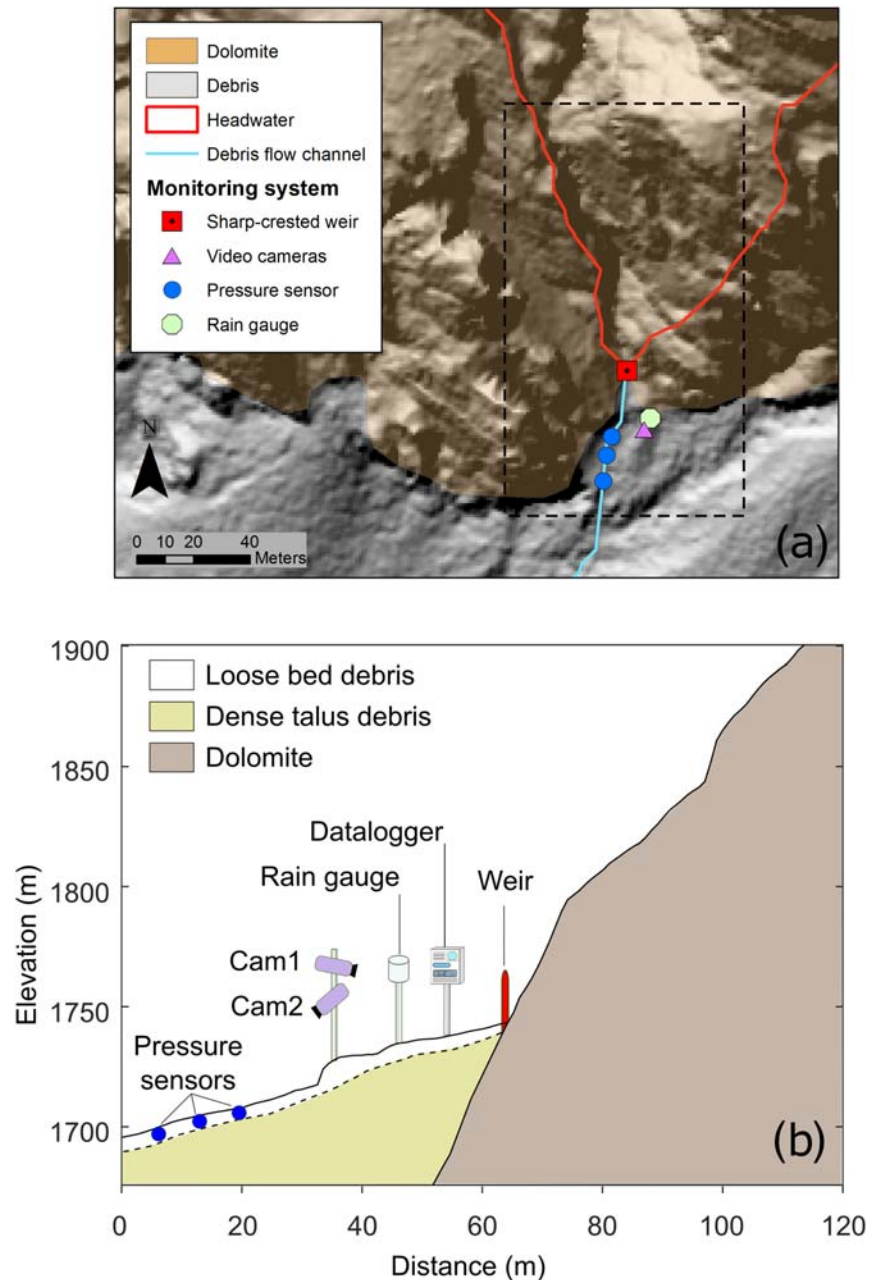
Figure 3. (a) Schematic map and (b) cross section of the monitoring system installed in the initiation area of the Dimai debris flow.

maintenance and extensive fieldwork to keep the stilling basin clear from debris and to repair the damages caused by transported rocks.

Three pressure sensors are located along the channel (about 50 m downstream the headwater outlet) to detect the occurrence of subsurface flow (Figure 4d). The sensors are buried into the bed debris at shallow depth (0.3–0.4 m) and were reinstalled several times because of the mobilization of the sediment bed. We initially installed vented sensors to have an automatic correction for the atmospheric pressure. However, the small vented tube that runs through the sensor cable was repeatedly damaged by the bedload transport, allowing the humidity to enter the tube and corrupting the measurements. Therefore, in 2013, we replaced the vented transducers with absolute pressure sensors. A barometer located in the data logger housing (Keller PAA-26W, 0.8–1.2 bar) provides data for atmospheric correction.

Figure 4. Pictures of the monitoring system: (a) general view of the area; (b) sharp-crested weir built at the outlet of the headwater catchment; (c) monitoring station; (d) upper reach of the debrisflow channel. Video cameras were originally installed on a pole located on the left bank of the channel (d); in 2014, we moved the camera further away from the channel (c) to prevent damages.

All the data are collected by a Campbell Scientific CR800 data logger (Figure 4c). The data logger scans the sensors every 1 s, checking the cumulated rainfall in the previous 5 min. In "no-event" mode, the logger stores the data every 5 min in the internal memory (4-MB capacity) and keeps the video cameras off. When the rainfall exceeds the threshold of 0.6 mm in 1 min (defined based on our previous experience in the area; Berti & Simoni, 2005), the system switches into "event" mode: data are recorded every 5 s on an external flash memory (2-GB capacity), and the video cameras are turned on. This threshold is well below the typical rainfall threshold for debris flow triggering in the area, and it was used to document the hydrologic behavior of the catchment in response to a large number of storms. The "event" mode lasts for 2 hr, then the system goes back in the "no-event" mode. However, if during this period the threshold is exceeded again, the timer resets, and the "event mode" restarts from that moment for another 2 hr. Power to the system comes from two 12-V 14-Ah batteries in parallel recharged by a 60 W solar panel.

The monitoring system worked for six debris flow seasons (from June to October) in years 2010, 2011, 2012, 2013, 2014, 2015, and 2016. During this period, we recorded 454 rainfall events (160 of which switched the system into the "event mode" activating the video cameras) and five debris flows (see section 4). Then, the system was destroyed by a major rockfall in summer 2017. During the period of operation, the monitoring system required continuous maintenance and ongoing repairs due to the harsh site conditions. Sensors and cables were frequently damaged by runoff flows and rockfalls, and the power system struck by lightings during violent thunderstorms. Remote control and periodic field surveys were fundamental to check the integrity of the system and to minimize data loss.
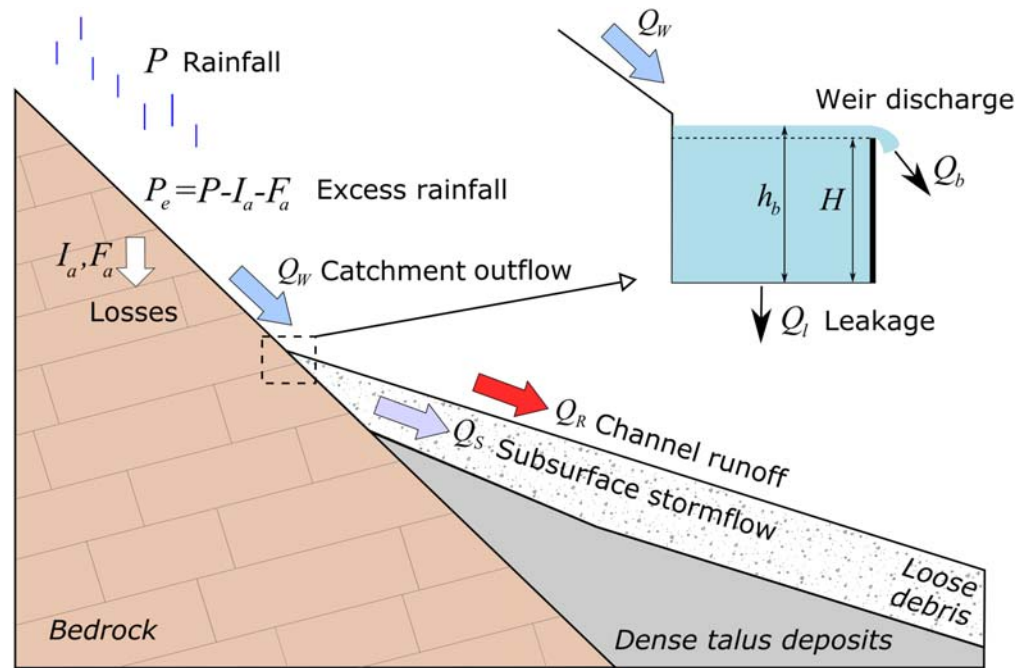
Figure 5. Conceptual model that describes the hydrologic behavior in the initiation area of a runoff triggered debris flow (modified from Berti & Simoni, 2005).

3.2. Data Analysis

Data analysis is based on the conceptual model for debris flow initiation proposed by Berti and Simoni (2005). The model describes the hydrologic response in the source area of a debris flow initiated by channel runoff, and it was developed for a similar catchment in the Dolomites. According to this model (Figure 5), a debris flow is triggered when the outflow discharge from the headwater rocky catchment (Q_W) exceeds the drainage capacity of the channel bed (Q_S) and generates surface channel runoff (Q_R). Debris flows then result from the progressive bulking of storm runoff with sediment eroded from the channel bed. The triggering criterion adopted by the authors requires a clarification. It is widely known that sediment motion in mountain channels occurs when the near-bed fluid stress exceeds a critical value, which mainly depends on bed slope and particles diameter (Prancevic et al., 2014; Takahashi, 1978). Therefore, a critical surface discharge is commonly required to initiate a debris flow (Gregoretti & Dalla Fontana, 2008; Tognacca et al., 2000). The simple model proposed by Berti and Simoni (2005) does not consider any critical discharge; thus, any time surface flow is generated ($Q_R>0$), a debris flow should occur. The authors justified this assumption by showing that, in the studied catchment, the critical discharge is small and that "a limited surface runoff of few centimeters" is enough to start bed mobilization. We will discuss this assumption further in sections 5 and 6.

3.2.1. Rainfall

The first step in the analysis is the identification of the rainfall events. Ideally, a rainfall event is a period of continuous precipitation well separated from other rainy periods (Melillo et al., 2015). In most cases, however, rainfall is a complex signal exhibiting fluctuations and an irregular behavior at multiple temporal scales, which makes an objective identification difficult. A common criterion is to define a minimum duration (D_{min}) and depth (P_{min}) of the no-rainfall period: a new event is then any rainfall measured after a no-rainfall period (Postance et al., 2017). The values of D_{min} and P_{min} depend on the different geological and hydrogeological conditions. A short interevent time is generally used for shallow landslides and debris flows which quickly respond to rainfall (e.g. Saito et al., 2010; Staley et al., 2013), while a long interevent time is adopted for deep-seated landslides in low-conductivity soils whose stability is affected by prolonged rainfall periods (e.g. Berti et al., 2012; Brunetti et al., 2010).

In our case, the catchment is very steep, the loose debris is highly conductive, and the evaporation rate is very high in summer. Both video footage and sensor data show that the catchment response to rainfall is
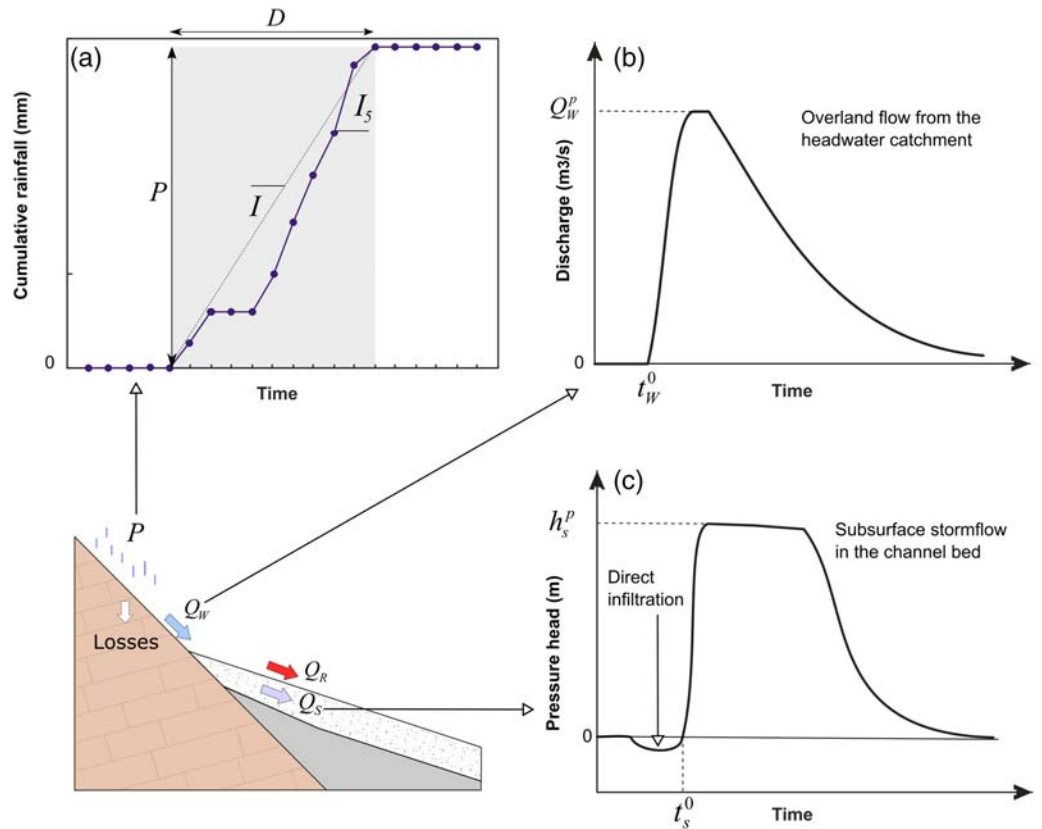
Figure 6. Parameters used for the analysis: (a) rainfall depth (P), rainfall duration (D), average intensity (I), and peak 5-min rainfall rate (I_5); (b) start (t_w^0) and peak discharge (Q_W^P) of the catchment outflow hydrograph; (c) arrival time (t_s^0) and peak pressure head (h_s^p) of the subsurface storm flow in the channel bed.

very fast (in the order of several minutes) and that the basin returns to the initial conditions in a few hours after the end of the rain. Therefore, we used a short interevent time ($D_{min} = 1$ hr) and a small rainfall depth ($P_{min} = 0.2$ mm) to separate rainfall events: a new rainfall event starts when the rainfall depth exceeds 0.2 mm in 1 hr and stops when rainfall goes below this threshold. The same criterion was used for critical and noncritical rainfall. Each rainfall event was then characterized by the rainfall depth (P), rainfall duration (D), average intensity ($I = P/D$), and peak 5-min rainfall rate (I_5) as shown in Figure 6a.

3.2.2. Outflow from the headwater catchment

The water level measured in the weir-stilling basin (h_b) was used to compute the outflow discharge from the rocky catchment (Q_W) (Figure 5). Q_W was calculated by the continuity equation:

$$Q_W(t) = \frac{dV_b}{dt} + Q_l + Q_b, \tag{1}$$

where dV_b/dt is the rate of change in time of the water volume within the stilling basin, $Q_l \approx 0.6 \cdot 10^{-4}$ m^3/s is the leakage through the weir bottom (which was not perfectly sealed), and Q_b is the discharge over the sharp-crested weir when h_b exceeds the weir height H:

$$Q_b = C_D B_E \sqrt{2g}(h_b - H)^{3/2}. \tag{2}$$

The discharge coefficient C_D and the effective weir width B_E are equal to 0.4 and $1.55 - 0.1(h_b - H)$, respectively (Gregoretti et al., 2016). The rate of change of the water volume dV_b/dt can be approximated by the backward difference of the stages recorded at 5-min interval:

$$\frac{dV_b}{dt} \approx \frac{\Delta V_b}{\Delta t} = \frac{V_b(i) - V_b(i-1)}{5 \cdot 60} = \frac{A_b h_b(i) - A_b h_b(i-1)}{5 \cdot 60}, \tag{3}$$

where $i = 1,..N$, N is the data index, $A_b = 3.72$ m^2 is the area of the stilling basin, and $\Delta t = 5 \cdot 60$ is the sampling rate in seconds. The error in dV_b/dt associated to the 1-mm accuracy of the pressure sensor is on the order of 1 L/s (Gregoretti et al., 2016). However, a much larger error may arise from the unknown flow density or because of the transported sediment, although this error is difficult to quantify.

Gregoretti et al. (2016) performed a detailed hydrological analysis of six hydrographs recorded at Dimai. They combined the Soil Conservation Service Curve Number (SCS-CN) procedure with a simplified version of the Horton equation and used a matched diffusivity kinematic wave model to route the excess rainfall and reproduce the observed hydrographs. Such an in-depth analysis is outside the scope of this research. We used weir data only to classify the storms; therefore, we just considered two hydrograph parameters: the start of the rising limb (t_W^0) and the peak outflow discharge (Q_W^p) (Figure 6b).

3.2.3. Subsurface Stormflow in the Channel Bed

The water collected by the headwater catchment quickly enters the debris flow channel. Here, the large pores of the loose debris allow the water to percolate down to a depth of 0.5–1 m, where the infiltration is impeded by the presence of dense slope debris. The formation of a perched zone of saturation at the top of this impending layer creates the condition for lateral flow through the connected pores and macropores of the bed sediment (Q_s in Figure 5). The pressure sensors buried into the channel bed allow detecting this subsurface stormflow.

Unfortunately, the heterogeneity of the debris and the presence of preferential flow through macropores do not allow to measure accurately the subsurface discharge Q_s. Therefore, the data collected by the pressure sensors were only used to evaluate the occurrence (presence and timing) of subsurface water. Figure 6c shows a typical sensor response and the parameters used to describe it. The initial drop of pressure head below zero is caused by the vertical infiltration of rainwater during the rainfall that wets the soil around the sensor tip. Since our sensors cannot measure soil suction, these values are meaningless. The sudden increase of pressure head above zero denotes the arrival of saturated subsurface flow. The pressure response usually resembles a trapezoid wave with steep rising limb, a pseudo-stationary peak stage, and a steep falling limb. Each pressure response was characterized by picking up the arrival time of the subsurface flow (t_s^0) and the peak pressure head (h_s^p) (Figure 6c).

3.2.4. Channel Runoff

Time-lapse videos were watched frame by frame to detect the appearance of surface water at the outlet of the rocky basin (*cam1*) and in the debris flow channel (*cam2*). Video images allowed us to recognize even just a trickle of water in the channel and to capture the time of appearance with an accuracy of a few seconds. Unfortunately, several storms occurred at night and could not be captured by the cameras. In these cases, we compared any available images before and after the rainfall event to check for signs of surface flow (erosion, deposition, and shifted boulders). We also made several attempts to estimate the flow depth and velocity using image analysis. However, the irregular channel morphology, the turbulent flow, and the erratic flow paths make these measurements impractical.

3.3. Hydrological Modeling

A simple hydrological model was developed to simulate the response to rainfall in the initiation area of the debris flow and to support the physical interpretation of the rainfall thresholds. The aim of the model is to estimate the peak runoff in the debris flow channel caused by rainfall of different duration and intensity. The model relies on the continuity principle:

$$Q_R = Q_W - Q_S, \tag{4}$$

that is, channel runoff (Q_R) results from the catchment outflow (Q_W) minus the water drained by subsurface stormflow (Q_S). The flow chart in Figure 7 and the explanation below illustrate the steps in the analysis.

3.3.1. Excess Rainfall in the Headwater Catchment

During a rainfall event, only part of the rain will contribute to the streamflow at the outlet of the headwater catchment. The excess rainfall (P_e) is the portion of total rainfall (P) that remains after initial (I_a) and continuing (F_a) abstractions and that runs as sheet flow over the cliffs. From the continuity principle:
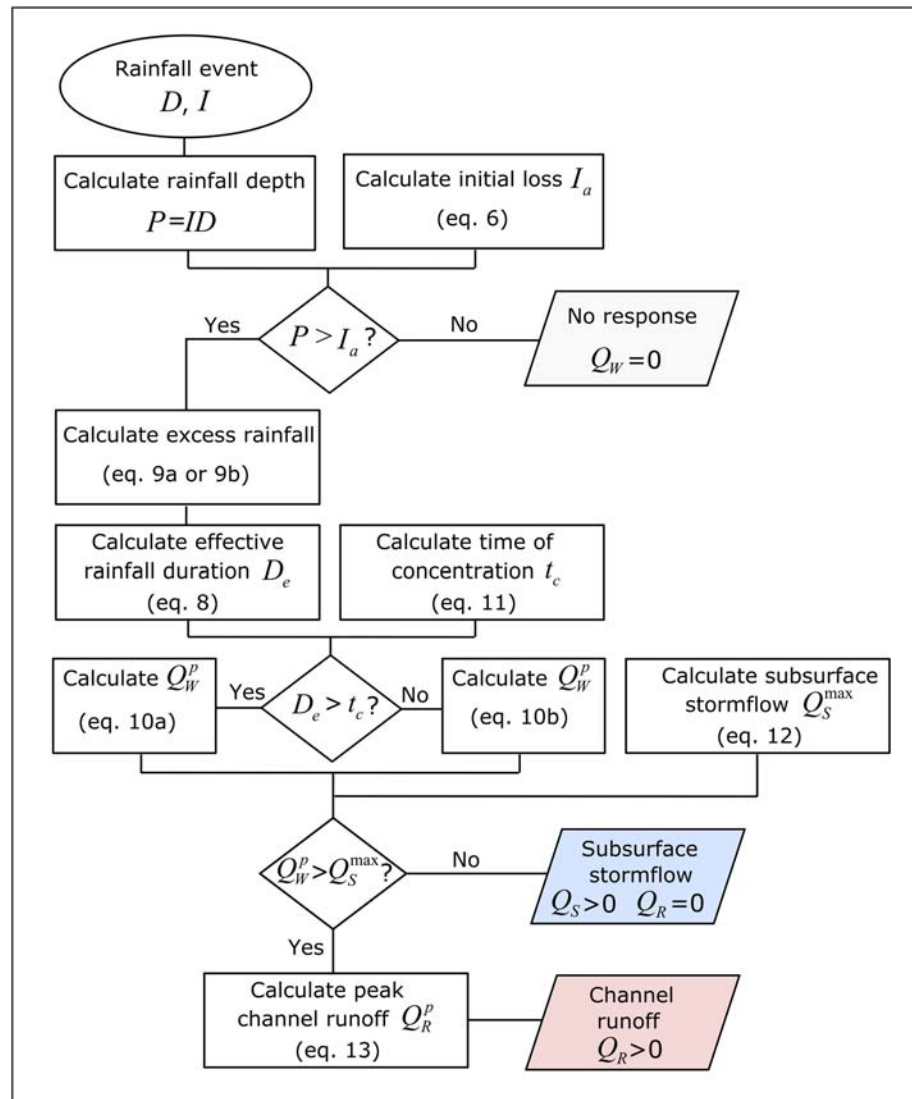
Figure 7. Flow diagram of the steady-state model used to simulate the response to rainfall in the initiation area of the debris flow.

$$P_e = P - I_a - F_a, \tag{5}$$

where all the quantities can be expressed in mm.

Initial abstractions (I_a) include rainfall lost to interception, depression storage, and wetting of the rock surface of the headwater catchment. Continuing abstractions (F_a) occur after runoff begins and mostly consist of percolation through the fractured rock.

Initial abstractions are estimated using the SCS-CN method (Soil Conservation Service, 1972), which has proved to be suitable to simulate runoff volume in steep rocky catchments of the Dolomites (Gregoretti et al., 2016; Gregoretti & Dalla Fontana, 2008). According to the model,

$$I_a = \lambda S, \tag{6}$$

where S is the maximum potential retention of the watershed (in inch) and λ is the initial abstraction ratio (normally set to a constant value $\lambda = 0.2$). The maximum potential retention is expressed as

$$S = \frac{1,000}{CN} - 10, \tag{7}$$

where Curve Number (CN) is a dimensionless catchment parameter ranging from 0 to 100, which mainly depends on soil type, vegetation, and antecedent moisture conditions (Soil Conservation Service, 1972).

Surface flow starts when the rainfall depth exceeds the initial loss ($P > I_a$). The time water begins to pond on the ground surface is called ponding time (t_e) and for a steady rainfall of duration D, and intensity I is simply given by $t_e = I_a/I$. By subtracting the ponding time from the storm duration, we obtain the duration of the excess precipitation (D_e):

$$D_e = D - \frac{I_a}{I}, \tag{8}$$

In order to calculate excess rainfall intensity ($I_e = P_e/D_e$), we need to estimate continuing abstractions (F_a). There are a number of methods available to estimate F_a. We consider two loss models commonly used for small catchments: the Constant Loss Rate and the SCS-CN models (Chow et al., 1988). In the first model, the total rainfall is reduced by a constant loss rate f_c, so continuing abstractions are simply $F_a = P - I_a - (I - f_c)D_e$. The second model assumes that the ratio of actual retention to potential retention (F_a/S) is equal to the ratio of actual runoff to potential runoff ($P_e/(P - I_a)$), then $F_a = SP_e/(P - I_a)$. The excess rainfall intensity predicted by the two model is therefore:

$$(1) \quad Constant\ Loss\ Rate, f_c: \quad I_e = (I - f_c). \tag{9a}$$

$$(2)\ SCS - CN\ abstractions: I_e = \frac{P_e}{D_e} = \frac{I(DI - I_a)}{DI + I_a\frac{(1-\lambda)}{\lambda}}. \tag{9b}$$

3.3.2. Catchment Outflow

The flow at the catchment outlet (Q_W) is obtained by routing the excess rainfall to the outlet. Because of the exposed bedrock and steep slopes, we can reasonably assume that surface flow is mainly the overland flow. The kinematic wave approximation of the Saint-Venant equation is suitable for routing flows in steep catchments and admits analytical solutions for overland flow over a uniform plane under constant rainfall rate (Singh, 1996). In these conditions, the peak outflow discharge (Q_W^p) depends on the duration of the excess rainfall (D_e) compared to the time of concentration (t_c) of the catchment:

$$Q_W^p = \frac{\sqrt{S_0}}{n}W(I_eD_e)^m \qquad if\ \ D_e < t_c, \tag{10a}$$

$$Q_W^p = WLI_e \qquad if\ \ D_e > t_c, \tag{10b}$$

where I_e is the excess rainfall intensity; L, W, and S_0 are the length, width, and slope of the catchment (modeled as a uniform plane); n is the Manning's roughness coefficient; m is a geometric parameter equal to 5/3 for turbulent overland flow (Linsley et al., 1982). The time of concentration can be calculated from the kinematic wave formula (t_c in minutes; Singh, 1996):

$$t_c = 6.94\frac{L^{0.6}n^{0.6}}{I_e^{0.4}S_0^{0.3}}, \tag{11}$$

or using one of the empirical equations available in the literature (Chow et al., 1988).

Equations 10a and 10b simply state that the maximum outlet discharge occurs when the effective storm duration equals or exceeds the time of concentration of the catchment ($D_e > t_c$): in this case, the entire drainage basin contributes to the flow and the peak discharge is given by the rate of excess rainfall multiplied by basin area (10b). If the storm duration is less than the time of concentration ($D_e < t_c$), the rain will cease before the maximum possible discharge is attained (10a).

3.3.3. Subsurface Drainage in the Channel

Part of the flow entering the channel drains out as subsurface flow (Q_S). The maximum value of Q_S is achieved when the bed layer is completely saturated; therefore, we can use the simple formula for steady-state, fully saturated, slope-parallel flow to get a rough estimate of the drainage capacity of the channel bed (Berti & Simoni, 2005; Beven, 1981):
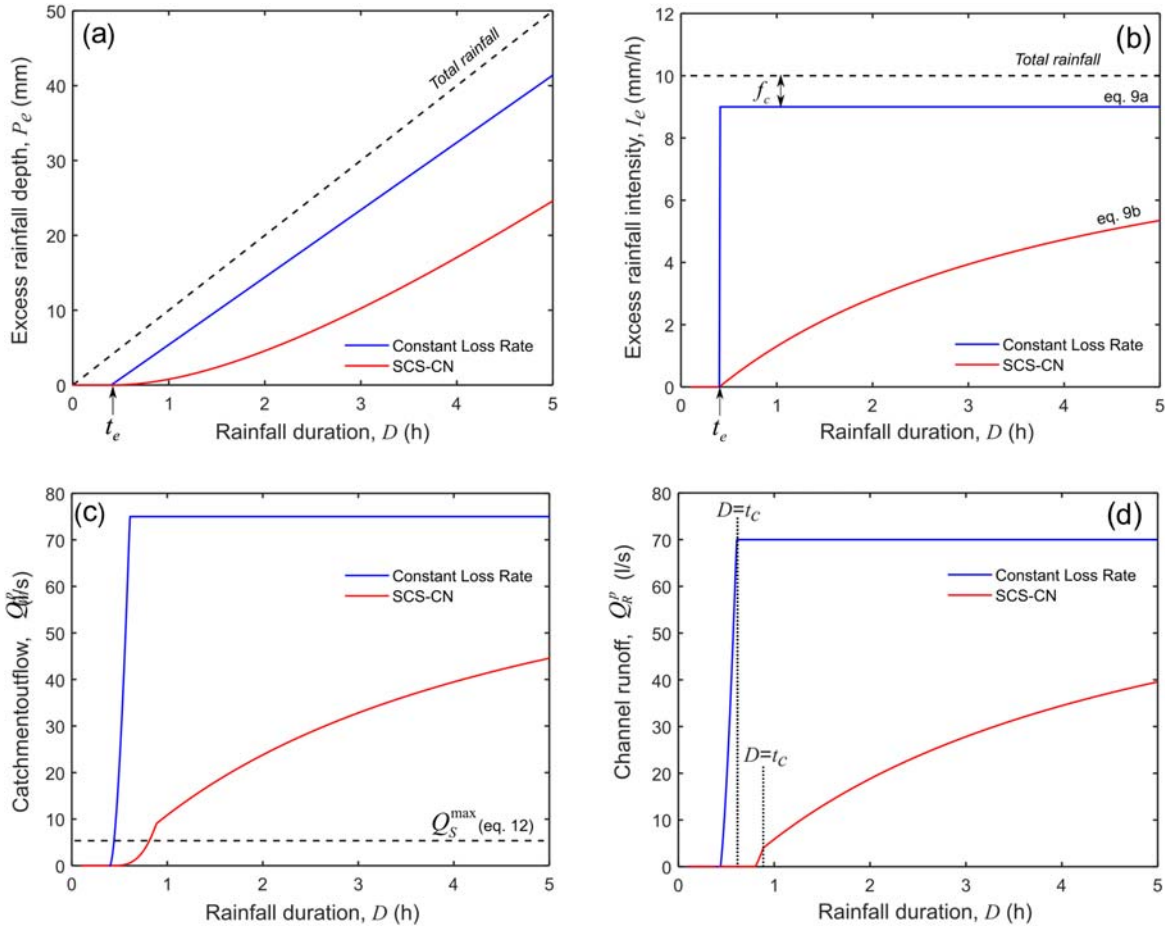
Figure 8. Example application of the hydrological model illustrated in Figure 7 (see text for details): (a) excess rainfall depth; (b) excess rainfall intensity; (c) peak surface flow at the outlet of the head water catchment; (d) peak surface runoff in the debris flow channel. The dashed lines in (a) and (b) indicate respectively the depth and intensity of the total rainfall. The dashed line in (c) indicates the maximum drainage capacity of the channel bed ($Q_S^{\max}$). t_e = ponding time. f_c = constant loss rate. f_c = time of concentration of the headwater catchment. Channel runoff in (d) is computed using equation (10a) for $D_e < t_c$ and equation (10b) for $D_e > t_c$. t_c is different for the two loss models because it depends on excess rainfall intensity (equation 11).

$$Q_S^{\max} = BHK\sin\theta, \tag{12}$$

where B is the channel width, H is the bed thickness, θ is the bed slope, and K is the saturated hydraulic conductivity of the sediment bed.

3.3.4. Channel Runoff

The maximum runoff discharge in the debris flow channel (Q_R^p) is finally obtained by substituting 10a and 12 in the continuity equation 4:

$$Q_R^p = Q_W^p - Q_S^{\max}. \tag{13}$$

Note that Q_R^p is the peak liquid discharge in the initiation area, not the critical runoff to initiate debris flow.

A sample application of the model is provided in Figure 8. The example considers the surface runoff generated at Dimai by storms with equal intensity ($I = 10$ mm/hr) and different duration (D = 0–5 hr). Model inputs are listed in Table 2. The first panel (Figure 8a) shows excess rainfall depth (P_e) calculated for the two considered loss models (Constant Loss Rate and SCS-CN). As expected, the excess rainfall is zero until the rainfall depth exceeds the initial loss ($P > I_a = 4$ mm), then it increases with storm duration D. However, the trend is different for the two models: the water available for runoff increases linearly with D in the Constant Loss Rate model and nonlinearly in the SCS-CN model. As a consequence, the excess rainfall intensity I_e (which is the slope of the $D - P_e$ curve) is constant in the first case and increases with D in the second (Figure 8b). Because of these differences in rainfall abstractions, the surface flow predicted by

Table 2
Input Parameters used to Simulate the Hydrologic Response to Rainfall in the Initiation Area of the Dimai Debris Flow

Headwater catchment		
	Length, L (m)[a]	300
	Width, W (m)	100
	Slope, S_0	1.7
	Initial abstractions, I_a (mm)	4
	Manning's coefficient, n	0.05
Channel bed	Width, B (m)	2.5
	Thickness, H (m)	0.5
	Slope, θ (°)	25
	Saturated hydraulic conductivity, K (m/s)	1E-2

[a]Linear distance from the divide to the outlet.

the two loss models at the catchment outlet (Figure 8c), and in the debris flow channel (Figure 8d) is different. Excess rainfall intensity is in fact the most important parameter in the runoff generation process and directly controls the amount and timing of surface flow.

4. Results

4.1. Rainfall

Over the monitoring period (six debris flow seasons from 2010 to 2016), we recorded 454 rainfall events. Most of them are short-duration convective thunderstorms resulting from the rapid vertical movement of unstable air masses which produce locally intense convective rainfall (Bernard et al., 2019; Underwood et al., 2016).

Figure 9 shows the frequency distributions of rainfall depth, duration, and intensity for the recorded events. Data are evenly distributed on a log scale and roughly follow a Weibull distribution with a shape factor of 1. About 80% of the events have a duration less than 3 hr and produce less than 10 mm of rain (Figures 8a and 8b). However, 10% of these storms can be classified as heavy/torrential rainfall (rainfall intensity $I > 10$ mm/hr; UKMO, 2007) (Figure 9c). Despite being very short, most of the recorded events are characterized by sudden bursts of heavy rain that generally happen at the beginning of the storm. As shown in Figure 9d, the 5-min intensity measured during a burst is about twice the average rainfall intensity for 1-hr rainfalls and can be up to 5 times higher for rains lasting a few hours. About 25% of the data would be classified as heavy/torrential storm based on burst intensity.

All the rainfall events are plotted in Figure 10a as data points of rainfall duration vs. rainfall intensity. The purple lines on the chart are the Intensity-Duration-Frequency (IDF) curves (Koutsoyiannis et al., 1998) obtained by Extreme Value type 1 (Gumbel) distribution of the annual maxima series of the nearby meteorological station of Podestagno (located 2.5 km to the north). IDF curves allow for the estimation of the return period of an observed rainfall. Results show that 75% of the intense rainfall has a return period less than 2 years and only five storms exceed the 5-year recurrence time.

4.2. Hydrologic Response of the Headwater Catchment

The sharp-crested weir measures the water discharge at the outlet of the headwater catchment (Q_W). Despite the difficult site conditions, we successfully recorded the hydrologic response to 379 rainfall events. Most of these rains (253 events, 67% of the total) produced no overland flow in the headwater and therefore no discharge at the outlet ($Q_W = 0$). Another 126 rainfall events (33% of the total) lead to the generation of substantial overland flow that produced a measurable discharge at the catchment outlet ($Q_W > 0$).

Figure 10b shows the recorded rainfall classified according to the observed response. As can be seen, the rainfall that did not produce outflow ($Q_W = 0$) is well separated from those that produced outflow ($Q_W > 0$). This allows drawing a first rainfall threshold that identifies the occurrence of surface flow at the outlet of the headwater catchment (Catchment Outflow Threshold [COT]; see below). The peak discharge measured at the catchment outlet (Q_W^p) ranges from a few liters per second to over 100 L/s increasing with the severity of the storm (Figure 10b). The discrepancies that appear in the chart, where similar rainfall seems to give different values of Q_W^p, mainly depend on errors in rainfall measurement. Convective
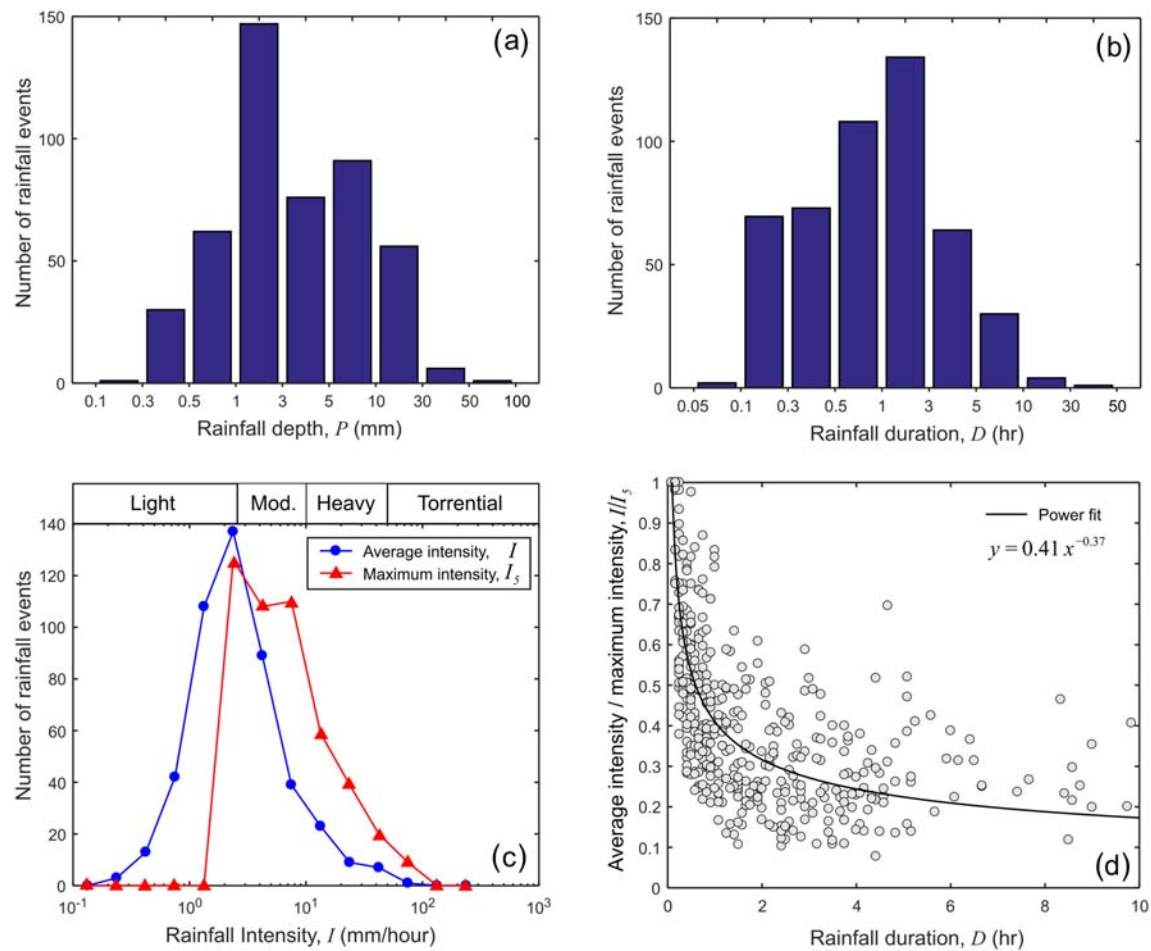
Figure 9. Characteristics of the 454 rainfall events recorded during the monitoring period: (a) frequency histogram of rainfall depth; (b) frequency histogram of the rainfall duration; (c) comparison of the frequency distribution of average and 5-min rainfall intensity; (d) relationship between rainfall duration and the ratio between average intensity and 5-min intensity. The intensity classes shown in (c) refer to the classification proposed by UKMO (2007).

thunderstorms are in fact highly localized in time and space and can hit only part of the catchment (Underwood et al., 2016). This can lead to large errors even in a small catchment.

The shape of the runoff hydrographs provides additional information on the hydrological behavior of the headwater. Typical hydrographs (Figures 11a and 11b) have a steep rising limb, while the falling limb is only slightly less steep, indicating that the catchment has limited storage capacity. Moreover, the flow rate changes rapidly during a storm and mimics the 5-min storm hyetograph (see, for example, Figure 11b). Such a direct connection between rainfall intensity and runoff rate proves that the time of concentration to the outlet is very short, in the order of a few minutes (see section 5).

4.3. Subsurface Stormflow in the Debris Flow Channel

Over the monitoring period, we recorded subsurface stormflow for 81 storms. Subsurface flow was clearly detected by the pressure sensors buried into the channel bed as a sudden increase of water level. Typical pressure response is rapid, transient, and characterized by steep rising limb followed by a plateau and a quick decrease (see the two examples in Figures 11c and 11d). In 80% of cases, the subsurface flow arrives at sensors location in less than 30 min after the beginning of the flow at the catchment outlet. Dividing the travel distance (about 50 m from the sensors location to the watershed outlet) by this lag time, and considering an average effective porosity of 0.3, leads to an estimate of the saturated hydraulic conductivity of the debris $K \approx 10^{-2}$ m/s. The coarse texture of the material and the presence of macropores explain such high conductivity values.
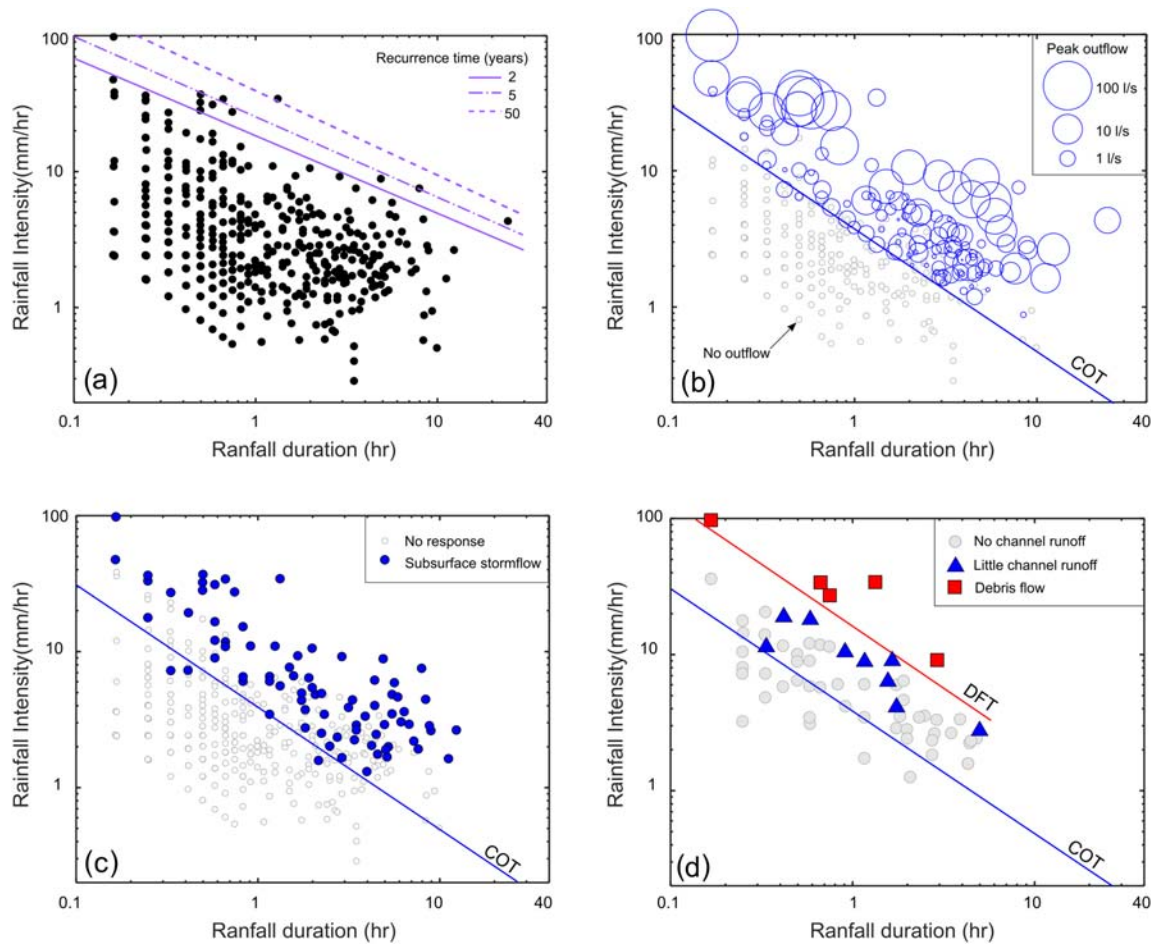
Figure 10. Analysis of the recorded rainfall events based the data of the monitoring system: (a) return period of the rainfall events (purple lines are the Intensity-Duration-Frequency curves calculated for the nearby meteorological station of Podestagno); (b) peak outflow discharge measured by the sharp-crested weir at the outlet of the headwater catchment; (c) classification of the rainfall events according to the presence of subsurface stormflow in the channel bed; (d) classification of the rainfall events according to the behavior observed in the videos. COT = Catchment Outflow Threshold. DFT = Debris Flow Threshold.

Figure 10c shows the rainfall events classified according to the sensors response ($Q_S = 0$: no response; $Q_S > 0$: subsurface stormflow). As can be seen, almost all the rainfall producing subsurface stormflow fall above the COT. This is expected, as the inflow to the channel is provided by headwater catchment, so it must be $Q_W > 0$ to have $Q_S > 0$. The data points that exceed the threshold without generating stormflow (gray circles above the threshold line in Figure 10c) are most likely "missed events," in which stormflow was actually generated but not intercepted by the sensors. Alternatively, they can be rainfall characterized by a high spatial variability that produces a large amount of rain at the rain gauge location but not in the headwater catchment.

4.4. Surface Runoff and Debris Flow Initiation

Critical conditions for debris flow mobilization occur when the catchment outflow largely exceeds the maximum drainage capacity of the channel bed ($Q_W >> Q_S^{max}$) leading to substantial runoff in the channel ($Q_R >> 0$). The video camera *cam2* captured the appearance of surface flow in the upper reach of the channel. During the monitoring period, we recorded approximately 190 hr of video in *cam2* (95 rainfall events × 2 hr), but we also missed 65 rainfall events because of power failures and damages caused by lightning strikes. Of the 95 recorded rainfall events, 27 happened at night (and the videos are too dark to use), 49 did not produce runoff, and 14 produced runoff (Figure 10d). In five cases, the runoff was strong enough to mobilize the bed sediment (red squares in the figure).

The videos recorded during these five storms document the initial stages of debris flows initiated by channel runoff. The water appears in the channel a few minutes after the start of the rain and increases rapidly. The
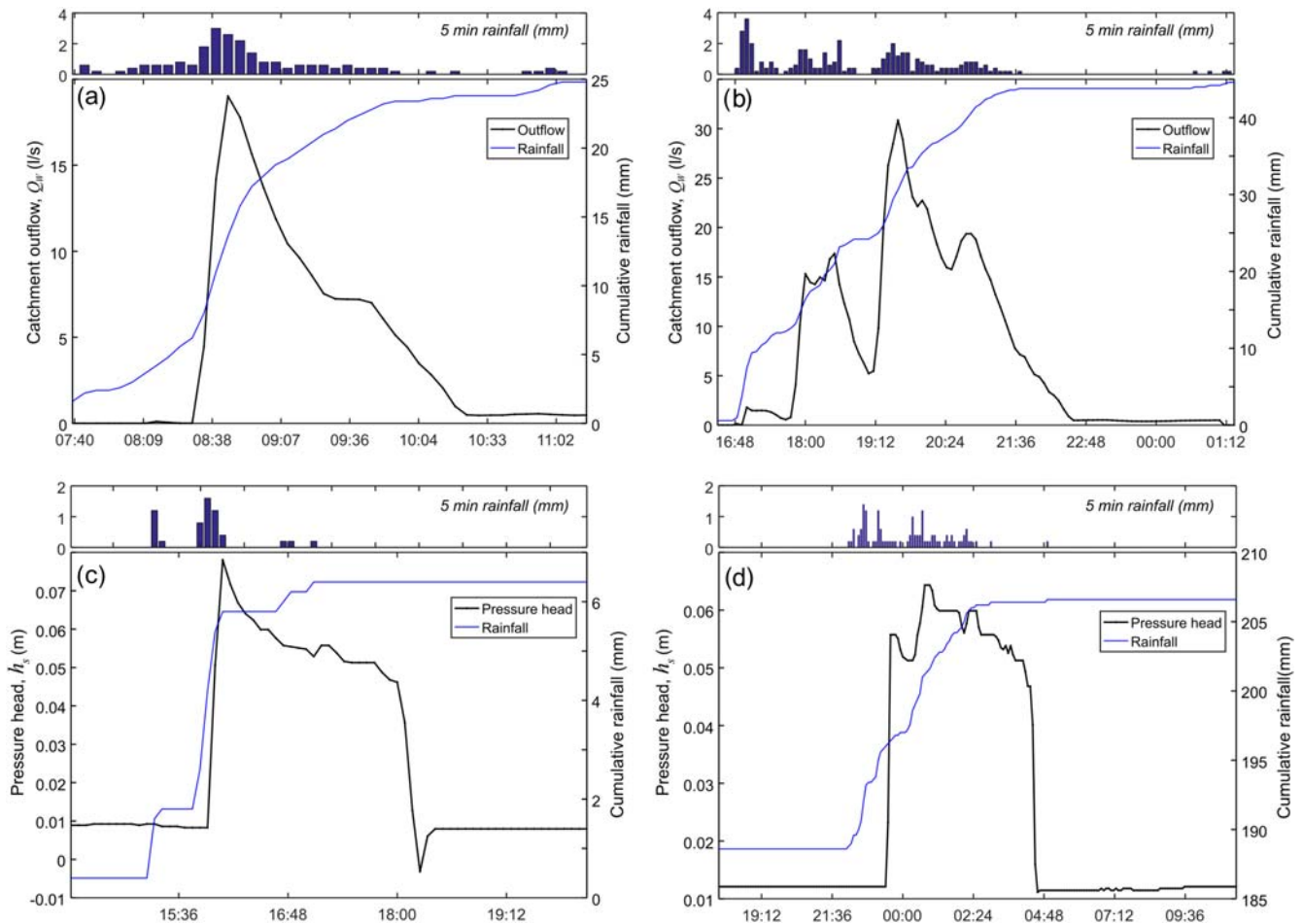
Figure 11. Sample data from the monitoring system: (a and b) surface flow at the outlet of the headwater catchment measured by the sharp-crested weir (a = 5 August 2016; b = 9 August 2016); (c and d) subsurface stormflow detected by the pressure sensors buried into the channel bed debris (c = 16 July 2011; d = 5 August 2011).

flow is fast, turbulent, and characterized by irregular fluctuations modulated by rainfall intensity. Massive erosion (from several centimeters up to few decimeters) occurs in the channel by entrainment of the material from the bed and, to a lesser extent, from the banks. The water is muddy brown due to the high sediment load and large blocks (up to 40–50 cm in diameter) that are transported downstream. The peak stage of the flow generally lasts 10–20 min with a maximum flow depth of about 20–40 cm. Then, the water level drops, the runoff rate reduces, and the erosion stops. In the initial stage, the debris flow is immature and looks like a concentrated mixture of water and sediment. Because of the turbulent murky water, it is not possible to tell if the sediment motion occurs "grain by grain" by progressive bulking or by mass failure of the bed (Prancevic et al., 2014). However, the formation of erosion furrows winding around big boulders and the incomplete submergence of the channel bed suggest that progressive bulking is the dominant mobilization mechanism.

The immature flow then increases its solid concentration and volume proceeding downstream, until it turns into a fully developed debris flows. Field surveys conducted after each event revealed the presence of typical debris flow deposits (internal levees, lateral levees, and deposition lobes) along the active channel pathway. Even the smaller events transformed into debris flows, although in this case, the material stopped just downstream of the initiation area. The observed behavior is typical for many headwater catchments in the Dolomites. In these catchments, debris flow is the dominant process by which bed sediment is transported along channels. Beadload or suspended transport generally does not occur: as soon as a critical discharge is exceeded, the sediment starts to mobilize, and a debris flow rapidly develops. This is consistent with the experimental findings of Gregoretti and Dalla Fontana (2008) showing that, at high slopes, the incipient
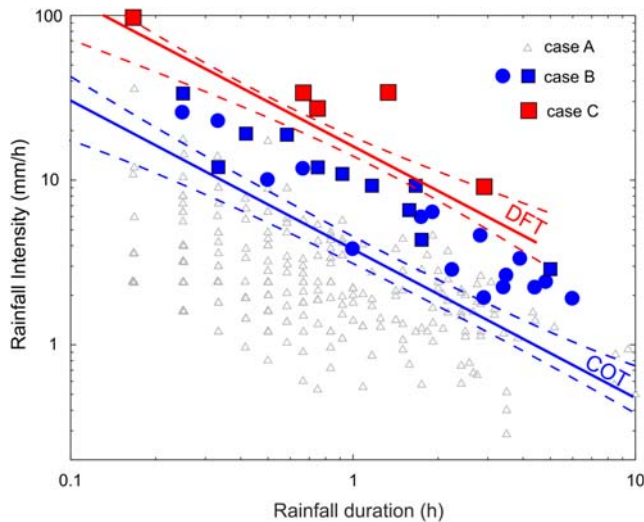
Figure 12. Hydrologic response in the initiation area of the Dimai debris flow. Case A = No response. Case B = Subsurface stormflow/little channel runoff (refer to text to see difference between blue dots and squares). Case C = Debris flow mobilization. COT = Catchment Outflow Threshold. DFT = Debris Flow Threshold.

motion condition coincides with the onset of high rate scouring and with the large entrainment of particles leading to a mass transport phenomenon.

Figure 10d compares the different responses to rainfall observed in *cam2* ($Q_R = 0$: no runoff; $Q_R > 0$: little runoff without bed erosion; $Q_R >> 0$: high runoff with debris flow mobilization). All the 14 rainfall events that produced channel runoff fall in the upper part of the diagram.

4.5. Rainfall Thresholds

The diagram in Figure 12 displays all the recorded storms in a single plot. Each storm is classified according to the observed hydrological response:

Case A   No response: all the rainwater is lost in the headwater catchment by infiltration or depression storage; there is no flow at the catchment outlet ($Q_W = 0$) and no flow in the debris flow channel ($Q_S = 0$, $Q_R = 0$).

Case B   Subsurface stormflow/little channel runoff: streamflow appears at the catchment outlet ($Q_W > 0$) but most of the water drains as subsurface flow without generating substantial runoff in the channel ($Q_S > 0$, $Q_R \simeq 0$).

Case C   Debris flow mobilization; the outflow from the headwater catchment far exceeds the drainage capacity of the channel bed, generating strong runoff in the debris flow channel ($Q_R >> 0$) and debris flow mobilization.

Two rainfall thresholds mark the transition between the three cases. The first threshold separates case A from B and defines the rainfall conditions to have streamflow at the outlet of the headwater catchment. We called this threshold COT. The COT is well defined by the weir data (Figure 10b) and plots as a straight line in the log *D*-log *I* plane. To find the equation of the separation line, we used a Linear Discriminant Analysis (LDA; Fisher, 1936; Rao, 1948). LDA is a statistical technique widely used in machine learning to find a linear combination of parameters that separates two (or more) classes of objects (Izenman, 2013). The analysis gives the following equation:

$$I = 3.8 \cdot D^{-0.9} \quad \text{Catchment Outflow Threshold (COT)}, \tag{14}$$

where *D* is in hours and *I* in mm/hr. The dashed blue lines in Figure 12 show the 95-percentile confidence interval around the COT. Rainfall above the COT satisfies the initial losses in the headwater and make water available for overland flow that enters the debris flow channel.

The second threshold separates case B from C. This is the usual Debris Flow Threshold (DFT) that defines the critical conditions for debris flow triggering. The DFT is less clearly defined because only five debris flows occurred during the monitoring period (Figure 10d). However, the five critical storms are well above the other 449 noncritical rainfall. According to the discriminant analysis, the DFT is roughly parallel to the COT but with a higher intercept:

$$I = 16 \cdot D^{-0.9} \quad \text{Debris Flow Threshold (DFT)}. \tag{15}$$

In this case, we cannot calculate the confidence interval because the sample size is too small. The red dashed lines in Figure 12 therefore indicate the range of variation of the DFT defined by the envelope of all the possible separation lines between B and C.

Case B deserves further comment. As can be seen in Figure 12, case B actually includes two different hydrological responses: storms that produce only subsurface stormflow (blue dots) and storms that generate subsurface flow and little surface runoff (blue squares). In principle, there should be a threshold between the two responses that identifies the limit conditions for which channel runoff starts to occur ($Q_W > Q_S^{max}$, so

$Q_R > 0$). Berti and Simoni (2005) used this limit condition to define the DFT at Acquabona. Our data do not show any clear separation between these two responses, although the rainfall generating runoff tends to be higher in the plot. This could be explained by many factors such as the moisture content of the debris at the time of the rainfall, the variable thickness of the bed layer, or simply the uncertainty in the true position of the data points due to the uncertainty in rainfall measurement.

5. Physical Interpretation of the Rainfall Thresholds

The data collected at Dimai provide a clear picture of the hydrology in the initiation area of the debris flow. Three different hydrological responses were observed, separated by two rainfall thresholds (Figure 12): the COT identifies the rainfall conditions for the generation of streamflow at the headwater outlet; the DFT identifies the initiation of debris flows by channel runoff. Both the thresholds can be expressed by power-law functions:

$$I = \alpha \cdot D^\beta, \tag{16}$$

where α is a scaling coefficient, β is the exponent of the power function, D is in mm, and I is in mm/hr. Equation 16 plots as a straight line on a log-log plot:

$$\log(I) = \log(\alpha) + \beta \cdot \log(D), \tag{17}$$

where β is the slope angle and $\log(\alpha)$ is the intercept, which corresponds to the value of rainfall intensity for $D = 1$ hr.

Rainfall thresholds commonly take the form of power-law functions (Guzzetti et al., 2007; Segoni et al., 2018; Staley et al., 2013), and because of the different conditions that trigger landslides in different regions, the parameters α and β can vary over a wide range. This introduces considerable uncertainty in threshold definition and makes any physical interpretation of these empirical relations very difficult. Our case is more favorable: (i) the data refer to a single catchment; (ii) the initiation mechanism is well defined; (iii) the two rainfall thresholds separate distinctive hydrological processes. Therefore, we can attempt a quantitative interpretation of the observed rainfall thresholds relying on simple hydrological concepts. The goal of this analysis is to explain the physical meaning of the parameters α and β in the specific case of debris flows triggered by surface runoff.

5.1. Catchment Outflow Threshold

Initial abstractions in the headwater catchment (I_a) are of particular interest in our case because they define a threshold value of rainfall that must occur before runoff is seen at the mouth of the catchment. Let us assume that a certain initial loss I_a is required to wet up the rock surface before runoff commences. In order to satisfy I_a, the rain depth must be $P = DI > I_a$. Therefore, the minimum value of rainfall intensity to have flow at the catchment outlet is

$$I = I_a \cdot D^{-1}, \tag{18}$$

or in log-form:

$$\log(I) = \log(I_a) - \log(D). \tag{19}$$

Equation 19 is a power-law function with $\alpha = I_a$ and $\beta = -1$. Mathematically, it represents the theoretical COT in the case of constant initial abstractions. From a physical perspective, it depicts a simple "bucket" model in which the headwater catchment acts like a barrel that collects the rainwater and spills out when the available storage has filled up.

This simple model seems to capture the essence of our empirical threshold. The slope of the COT is actually close to -1 ($\beta = -0.9$, but -1 is within the 95-percentile confidence interval shown Figure 12), and the intercept $\alpha = I_a = 3.8$ mm is a reasonable value for the initial losses in a steep rocky catchment. In fact, using the SCS-CN method (see section 3.3) and assuming typical values for steep, unvegetated rock slopes ($CN = 85$–90, and $\lambda = 0.1$; Gregoretti & Dalla Fontana, 2008), we obtain an estimate of $I_a = 2.8$–4.5 mm that closely agrees with the empirical value $\alpha = 3.8$ mm (Figure 13).
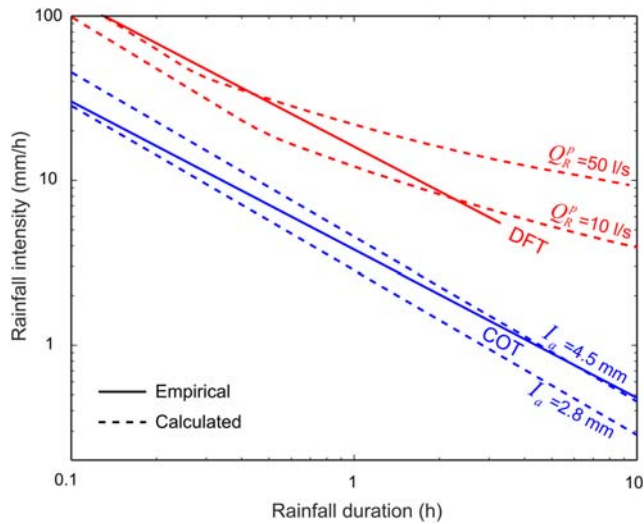
Figure 13. Comparison between empirical and calculated rainfall thresholds. The theoretical Catchment Outflow Thresholds (blue dashed lines) result from the simple "bucket" model of equation (19) using typical values of initial loss (I_a) for rock slopes. The theoretical Debris Flow Thresholds (red dashed lines) result from the hydrological model described in section 3.3 (Figure 7) using the input data in Table 2 (see also Figure 14b).

5.2. Debris Flow Threshold

A simple bucket model cannot explain the DFT because at Dimai debris flows are triggered when surface runoff exceeds a certain critical discharge. Therefore, we must route the excess rainfall over the catchment to estimate the surface discharge in the channel. To gain a physical explanation of the DFT we then need a rainfall-runoff analysis. The simple hydrological model described in section 3.3 is suitable for this purpose because it provides a physical framework for understanding the relationship between rainfall conditions and debris flow triggering.

The model calculates the peak runoff in the debris flow channel (Q_R^p) in response to a uniform rainfall of certain duration and intensity. We applied the model by considering 50×50 synthetic storms (logarithmically distributed in the range $D = 0.1$–30 hr, $I = 0.1$–100 mm/hr) and the catchment characteristics summarized in Table 2. Figure 14 shows the result of the analysis. The two diagrams refer to the different loss models employed to calculate excess rainfall in the headwater catchment (Constant Loss rate and SCS-CN). The three colored areas highlight the hydrological response predicted by the model (gray area = no response; blue area = subsurface flow; red area = channel runoff). The solid black lines connect points of equal runoff rate.

Both the loss models simulate the observed behavior of the catchment (compare Figure 14 with Figure 12), but they differ in predicting the critical conditions for debris flow triggering. The runoff curves calculated with the Constant Loss Rate model (Figure 14a) are essentially horizontal and cannot reproduce the sloping trend of the empirical DFT. This is because at Dimai storm durations are generally longer than the time of concentration of the catchment, which is in the order of 10–15 min (equation 11): in this condition, the entire catchment is contributing to the flow, and the outflow only depends on the excess rainfall intensity I_e (equation 10b). Since the Constant Loss Rate model assumes that I_e is independent of storm duration (equation 9a; see also the example in Figure 8), the runoff contours are horizontal.

The SCS-CN loss model provides better results (Figure 14b). In this case, the effective rainfall intensity increases with storm duration as predicted by equation 9b; therefore, long rainfall must be less intense to produce the same runoff. Consequently, the runoff contours show a negative slope that mimics the empirical threshold. The empirical threshold intersects the SCS contours with a runoff rate in the range 10–50 L/s. Similar values of flow rate are measured by the sharp-crested weir in the case of high-intensity storms that cause mobilization of the sediment bed (Figure 10b). Either of these two curves would therefore provide a reasonable approximation to the empirical DFT as shown in Figure 13. There is however an obvious difference between the thresholds: while the empirical threshold is a line, the modeled thresholds graph as curves (in the log-log space). Because of the different shape, the theoretical thresholds significantly deviate from the empirical one for storms lasting more than 3–4 hr. Such a discrepancy might indicate a poor model accuracy, but we must consider that the exact shape of the empirical threshold is actually unknown: only five debris flows occurred during the monitoring period, and the longest critical rainfall was about 3 hr. Moreover, most rainfall thresholds for the occurrence of debris flows are based on measurements of rainfall intensity over short duration (less the 1–3 hr; Staley et al., 2017; Segoni et al., 2018), so it is difficult to judge if the decreasing slope of the DFT is reasonable or not. Focusing on the critical storms, from a visual inspection of Figure 14, it looks like the five debris flows were triggered by peak runoff rates ranging from 10 to 200 L/s. These values agree well with the critical surface discharge computed using the empirical model proposed by Gregoretti and Dalla Fontana (2008). According to this model, the critical surface discharge should range from 7 to 170 L/s for a characteristic grain size of the sediment layer varying from 1 to 10 cm. The overall results show that, despite the simplified approach, the kinematic-wave model provides a quantitative framework to interpret the DFT and allows us to recognize the critical importance or rainfall abstractions in the hydrologic response of the catchment.
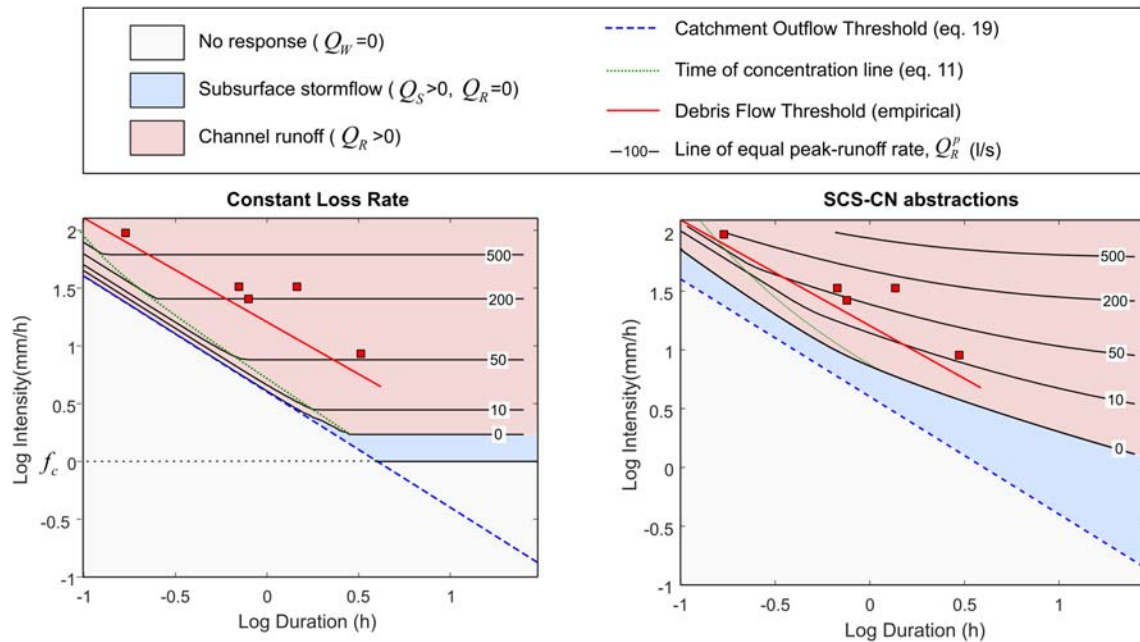
Figure 14. Application of the hydrological model described in section 3.3 (Figure 7) to Dimai. The two diagrams refer to the different loss models used to estimate excess rainfall (Constant Loss Rate and SCS-CN). The black curves connect points of equal-channel runoff. The gray area (no response) is bounded by the axes and by the theoretical Catchment Outflow Threshold, calculated assuming an initial loss $I_a = 4$ mm (equation 19). The blue area (subsurface flow) is bounded by the COT and by the runoff curve $Q_R^p = O$. The red area (Channel runoff) extends above the curve $Q_R^p = O$ and indicates the storms that generate a surface runoff in the debris flow channel.

6. Discussion

The analysis above suggests that a simple bucket model (equation 17) can explain both the slope and the intercept of the COT at Dimai. The intercept represents the initial losses in the headwater catchment ($\alpha = I_a$), while the slope is fixed ($\beta = -1$). This point deserves further discussion. The theoretical value $\beta = -1$ comes from the assumption that I_a is a fixed quantity, independent of the rainfall duration and intensity. While this assumption is reasonable for a small rock basin, it does not apply to catchments mantled by soils. In this case, the amount of water the soil can absorb is primarily determined by the infiltration rate of the ground (f), which changes as a function of rainfall intensity and varies with time during the event (Chow et al., 1988).

We can use standard infiltration equations to investigate how a time-varying infiltration rate will affect the theoretical value of β. Let us consider two models commonly used for predicting water infiltration, the Green-Ampt (Green & Ampt, 1911) and the Philip (Philip, 1957) methods. The Green-Ampt equation for potential infiltration rate is

$$f = \frac{\psi \Delta \theta K}{F} + K, \tag{20a}$$

where K is the saturated hydraulic conductivity, ψ is the wetting front suction head, $\Delta\theta$ is the change in moisture content across the wetting front, and F is the cumulative infiltration depth. The Philip equation is

$$f = \frac{1}{2} S t^{-0.5} + K, \tag{20b}$$

where t is time and S ($LT^{-1/2}$) is a soil parameter called sorptivity which measures the capacity of the soil to absorb or desorb water by capillarity. In both equations, the first term represents the effects of soil suction (that is the uptake of water by capillary forces), and the second term the gravity-driven vertical flow.

During a rainfall event, the potential infiltration rate is initially high due to the large suction gradient, then decreases exponentially with time approaching the saturated conductivity K. Excess rainfall (or ponding) begins when the rainfall rate equals the potential infiltration rate ($f = I$). In the special case of

short-duration rainfall over an initially unsaturated soil (a possible condition in debris flow catchments), the capillary flow dominates the infiltration process. Consequently, the minimum intensity for runoff generation can be obtained from (20a) and (20b) neglecting the gravity terms:

$$I = \sqrt{\frac{\psi \Delta \theta K}{2}} \cdot D^{-0.5} \quad \text{Green-Ampt,} \tag{21a}$$

$$I = \frac{1}{2} S D^{-0.5} \quad \text{Philip.} \tag{21b}$$

Storm duration in (21a) results from the integration of the function $f = \dfrac{dF}{dt} = \dfrac{\psi \Delta \theta K}{F}$, which brings $F = \sqrt{2\psi \Delta \theta K D}$ for $t = D$.

As can be seen, both equations predict a power-law relationship between I and D with rainfall intensity proportional to the square root of rainfall duration:

$$I \propto D^{-0.5}. \tag{22}$$

The theoretical slope of the threshold is therefore $\beta = -0.5$ in both cases. Interestingly, this suggests that the slope of the COT mainly depends on the land cover upstream of the initiation area: lower values are expected for soil slopes ($\beta \approx -0.5$), higher values for rock slopes ($\beta \approx -1$).

The analysis of the DFT confirms the critical importance of water abstractions. If the excess rainfall is calculated using a Constant Loss Rate model (which considers the catchment as a single storage with a constant leakage), it is not possible to reproduce the observed DFT (Figure 14a). Better results are obtained using a SCS-CN loss model (Figure 14b). This model considers the catchment as a nonlinear distribution of storages of various size (Priestley, 2015): large storages represent areas with high permeability, small storages areas with low permeability. Water abstractions are thus very high when the rainfall starts (because all the storages are empty) and level off with time as the storages fill. This explains why the runoff rate increases with storm duration even if the entire catchment is already contributing to the flow (equation 10b) and justifies the negative slope of the empirical threshold.

The drawing in Figure 15 illustrates the physical analog of our conceptual model. We can represent the process of rainfall-runoff transformation at Dimai with a chain of two cascading reservoirs. The first reservoir simulates the headwater catchment, and the second the stream channel bed. The rain falls into the first reservoir and accumulates at the bottom. When the rainfall depth exceeds the initial losses I_a, the water starts to spill out flowing to the outlet (COT). The outflow rate depends on rainfall duration (besides intensity) because storages of various sizes fill up in different times. The excess water then enters the second reservoir and partly flows out the bottom hole, which simulates the subsurface drainage throughout the bed. As predicted by equation 12, the rate at which water flows out of the hole depends on water table depth in the bed layer. Runoff occurs when there is more water from the first reservoir than the second reservoir can drain through the hole ($Q_w > Q_S^{max}$). This physical analog model is different from the "leaky-barrel model" commonly used to forecast landslide-triggered debris flows (Wilson & Wieczoreck, 1995). While the leaky-barrel model simulates the accumulation of water in the potentially unstable soil (the barrel), our analysis aims to predict the water that spills out of the barrel to simulate the excess rainfall available to runoff.

A last point of discussion is the portability of the model, that is, the possibility to predict the DFT at other sites. In principle, this is possible. All the parameters required for the analysis can be easily measured in the field or estimated by calibration from a limited number of events. There are however two important points to consider.

The first is the initiation process. At Dimai, the initiation is by "fireshose effect" (Johnson & Rodine, 1984); that is, the material is mobilized by a concentrated flow at the outlet of a steep rocky catchment; in this case, there is a sharp transition between talus and rock, and the initiation area is well defined. The situation is far more complicated in catchments where debris flows are initiated "by rilling" (Godt & Coe, 2007). Rills are common in steep, unvegetated slopes and form complex, highly connected distributary networks. In these catchments, debris flows are still mobilized by overland flow, but there is a gradual transition from clear
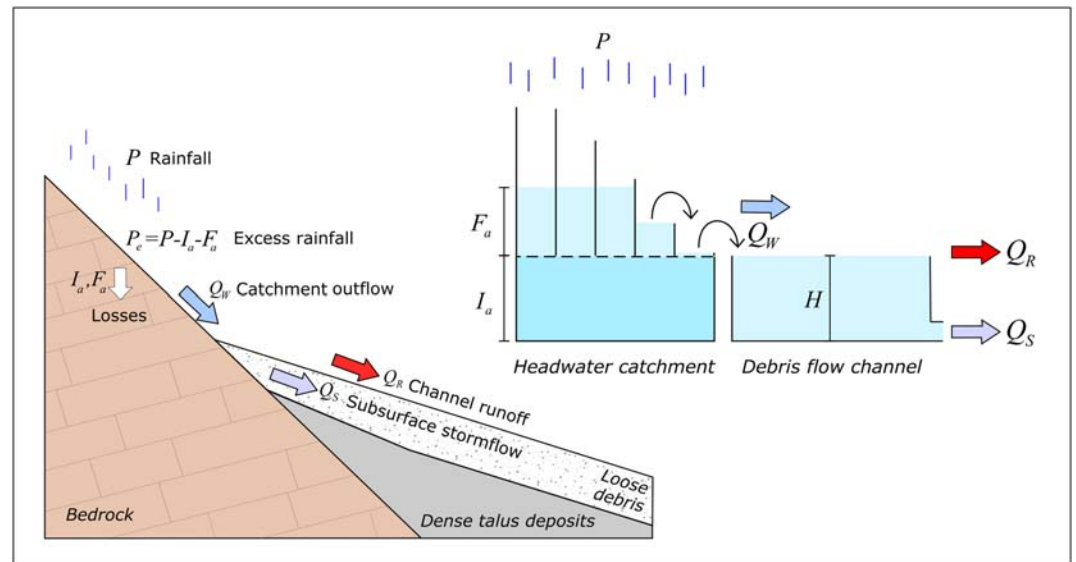
Figure 15. Physical analog that describes the hydrologic response in the initiation area of the Dimai debris flow. The model consists of a chain of two cascading reservoirs: the first simulates the headwater catchment, the second the debris flow channel (see text for explanation).

water flow to debris flow so it is difficult to identify the source areas. Extensive field surveys are necessary in this case to locate the starting point of the flows. Instead, we believe that the model does not apply where debris flows are triggered by en-mass failure of the sediment bed rather than progressive bulking. For instance, at Chalk Cliffs (Kean et al., 2013), surface water transports the sediment from steep channel reaches to lower gradient sections, creating temporary dams that can be overtopped by the incoming water causing the sudden release of the accumulated material. Such a complex process is not considered in our model; therefore, the method is probably not applicable.

The second point is the choice of the critical surface discharge. As you will recall, the model predicts the peak liquid discharge in the initiation area (equation 4), not the critical runoff for debris flow triggering. At Dimai, we estimated a critical discharge of 10–50 L/s by comparing the computed runoff rate with the empirical threshold (Figure 14). These values agree well with the surface discharge measured by the weir (Figure 10) and with the critical discharge predicted by the Gregoretti and Dalla Fontana (2008) model. This model (and others that are similar) can be used to estimate the critical surface discharge in areas with no historical data on debris flow occurrence. However, we advise caution when using these methods since the uncertainty associated with the input parameters can be very large. For operational purposes, it might be safer to define a conservative DFT using the runoff curve $Q_R = 0$, as proposed by Berti and Simoni (2005).

In conclusion, we encourage scientists to check the validity of the proposed approach in other catchments and to compare their empirical threshold with the one computed by the model. However, we recommend special caution when using the model for blind predictions in areas where field data and historical information on past debris flow activity are limited.

7. Conclusion

The following conclusions can be drawn from the current study.

1. Debris flows at Dimai are triggered by short-duration high-intensity storms, when the overland flow generated on the headwater catchment enters the debris flow channel causing surface runoff and the progressive entrainment of the sediment bed.
2. Field data show the existence of two rainfall thresholds: a lower threshold identifies the rainfall conditions for the generation of streamflow at the headwater outlet (COT); an upper threshold identifies the initiation of debris flows by channel runoff (DFT).

3. The COT can be explained by a simple "bucket" model; according to this model, the threshold line has a negative unit slope ($\beta = -1$), and the intercept represents the initial loss in the rocky headwater catchment ($\alpha = I_a$). Theoretical analyses show that in case of soil slopes, the threshold should have a slope $\beta = -0.5$.

4. The DFT can be satisfactorily reproduced using a simplified rainfall-runoff model in which the excess rainfall is routed over the headwater catchment using a kinematic-wave scheme. The critical parameter of the model is the water lost during the rainfall in the headwater catchment. Reasonable results are obtained employing the SCS-CN loss model, which considers the catchment as a non-linear distribution of storages of various size.

5. The overall behavior of the catchment is well captured by a physical analog which consists of a chain of two cascading reservoirs. The first reservoir simulates the headwater catchment, the second the stream channel bed. Unlike the "leaky-barrel model" commonly used to forecast landslide-triggered debris flows, this physical analog aims to predict the excess rainfall available to surface runoff rather than the water accumulating into the soil.

The quantitative analysis presented in this paper was made possible by the availability of long-term monitoring data and by the relatively simple hydrology of the Dimai catchment. However, the behavior observed at Dimai is typical of many catchments where debris flows are triggered by surface runoff. We therefore believe that our approach is of general validity and can be applied in other catchments to provide physically based rainfall threshold for the occurrence of runoff-generated debris flows.

References

Abancó, C., Hürlimann, M., Moya, J., & Berenguer, M. (2016). Critical rainfall conditions for the initiation of torrential flows: Results from the Rebaixader catchment (Central Pyrenees). *Journal of Hydrology*, *541*, 218–229.

Aleotti, P. (2004). A warning system for rainfall-induced shallow failures. *Engineering Geology*, *73*, 247–265.

Baum, R. L., & Godt, J. W. (2010). Early warning of rainfall-induced shallow landslides and debris flows in the USA. *Landslides*, *7*(3), 259–272.

Bernard, M., Underwood, S. J., Berti, M., Simoni, A., & Gregoretti, C. (2019). Observations of the atmospheric electric field preceding intense rainfall events in the dolomite Alps near Cortina d'Ampezzo, Italy. *Meteorology and Atmospheric Physics*, *132*, 99–111.

Berti, M., Genevois, R., Simoni, A., & Tecca, P. R. (1999). Field observations of a debris flow event in the Dolomites. *Geomorphology*, *29*, 265–274.

Berti, M., Martina, M. L. V., Franceschini, S., Pignone, S., Simoni, A., & Pizziolo, M. (2012). Probabilistic rainfall thresholds for landslide occurrence using a Bayesian approach. *Journal of Geophysical Research*, *117*, F04006. https://doi.org/10.1029/2012JF002367

Berti, M., & Simoni, A. (2005). Experimental evidences and numerical modelling of debris flow initiated by channel runoff. *Landslides*, *2*(3), 171–182.

Beven, K. J. (1981). Kinematic subsurface stormflow. *Water Resources Research*, *17*, 1419–1424.

Bosellini, A., Gianolla, P., & Stefani, M. (2003). Geology of the Dolomites. *Episodes*, *26*(3), 181–185.

Brunetti, M. T., Peruccacci, S., Rossi, M., Luciani, S., Valigi, D., & Guzzetti, F. (2010). Rainfall thresholds for the possible occurrence of landslides in Italy. *Natural Hazards and Earth System Sciences*, *10*, 447–458.

Cannon, S. H., Boldt, E. M., Laber, J. L., Kean, J. W., & Staley, D. M. (2011). Rainfall intensity-duration thresholds for postfire debris-flow emergency response planning. *Natural Hazards*, 209–236.

Cannon, S. H., Gartner, J. E., Wilson, R. C., Bowers, J. C., & Laberd, J. L. (2008). Storm rainfall conditions for floods and debris flows from recently burned areas in southwestern Colorado and southern California. *Geomorphology*, *96*, 250–269.

Chang, K. T., Chiang, S. H., & Lei, F. (2008). Analysing the relationship between typhoon-triggered landslides and critical rainfall conditions. *Earth Surface Processes and Landforms*, *33*, 1261–1271.

Chow, V. T., Maidment, D. R., & Mays, W. (1988). *Applied Hydrology*. New York: McGraw-Hill.

Chowdhury, R., & Flentje, P. (2002). Uncertainties in rainfall-induced landslide hazard. *Quarterly Journal of Engineering Geology and Hydrogeology*, *35*, 61–69.

Coe, J. A., Cannon, S. H., & Santi, P. M. (2008). Introduction to the special issue on debris flows initiated by runoff, erosion, and sediment entrainment in western North America. *Geomorphology*, *96*(3–4), 247–249.

Coe, J. A., Kinner, D. A., & Godt, J. W. (2008). Initiation conditions for debris flows generated by runoff at Chalk Cliffs, central Colorado. *Geomorphology*, *96*(3–4), 270–297.

Corominas, J., van Westen, C. J., Frattini, P., Cascini, L., Malet, J. P., Fotopoulou, S., & Smith, J. T. (2014). Recommendations for the quantitative analysis of landslide risk. *Bulletin of Engineering Geology and the Environment*, *73*(2), 209–263.

Cruden, D. M., & Varnes, D. J. (1996). Landslide types and processes. In A. K. Turner, & R. L. Shuster (Eds.), *Landslides: Investigation and Mitigation* (Vol. 247, pp. 36–75). Washington: National Academy Press.

Fisher, R. A. (1936). The use of multiple measurements in taxonomic problems. *Annals of Eugenics*, *7*(2), 179–188.

Fusco, F., De Vita, P., Mirus, B. B., Baum, R. L., Allocca, V., Tufano, R., & Calcaterra, D. (2019). Physically based estimation of rainfall thresholds triggering shallow landslides in volcanic slopes of southern Italy. *Water*, *11*(9), 1–24.

Giannecchini, R., Galanti, Y., & D'Amato Avanzi, G. (2012). Critical rainfall thresholds for triggering shallow landslides in the Serchio River Valley (Tuscany, Italy). *Natural Hazards and Earth System Sciences*, *12*, 829–842.

Godt, J. W., & Coe, J. A. (2007). Alpine debris flows triggered by a 28 July 1999 thunderstorm in the central front range, Colorado. *Geomorphology*, *84*, 80–97.

Green, W. H., & Ampt, G. A. (1911). Studies on soil physics. *The Journal of Agricultural Science*, *4*(1), 1–24.

Gregoretti, C., & Dalla Fontana, G. (2008). The triggering of debris flow due to channel-bed failure in some alpine headwater basins of the Dolomites: Analyses of critical runoff. *Hydrological Processes*, *22*, 2248–2263.

Gregoretti, C., Degetto, M., Bernard, M., Crucil, G., Pimazzoni, A., De Vido, G., et al. (2016). Runoff of small rocky headwater catchments: Field observations and hydrological modeling. *Water Resources Research*, *52*, 8138–8158. https://doi.org/10.1002/2016WR018675

Guo, X. J., Cui, P., & Li, Y. (2013). Debris flow warning threshold based on antecedent rainfall: A case study in Jiangjia Ravine, Yunnan, China. *Journal of Mountain Science*, *10*, 305–314.

Guzzetti, F., Peruccacci, S., Rossi, M., & Stark, C. P. (2007). Rainfall thresholds for the initiation of landslides in central and southern Europe. *Meteorology and Atmospheric Physics*, *98*, 239–267.

Huang, J., Ju, N. P., Liao, Y. J., & Liu, D. D. (2015). Determination of rainfall thresholds for shallow landslides by a probabilistic and empirical method. *Natural Hazards and Earth System Sciences*, *15*(12), 2715–2723.

Hungr, O., Evans, S. G., Bovis, M. J., & Hutchinson, J. N. (2001). A review of the classification of landslides the flow type. *Environmental and Engineering Geoscience*, *7*(3), 221–238. https://doi.org/10.2113/gseegeosci.7.3.221

Hürlimann, M., Abancó, C., Moya, J., & Vilajosana, I. (2014). Results and experiences gathered at the Rebaixader debris-flow monitoring site, Central Pyrenees, Spain. *Landslides*, *11*, 939–953.

Hutchinson, J. N. (1988). General report: Morphological and geotechnical parameters of landslides in relation to geology and hydrogeology. Paper presented at Fifth International Symposium on Landslides, Rotterdam, Netherlands.

Iadanza, C., Trigila, A., & Napolitano, F. (2016). Identification and characterization of rainfall events responsible for triggering of debris flows and shallow landslides. *Journal of Hydrology*, *541*, 230–245.

Iverson, R. M. (1997). Physics of debris flow. *Reviews of Geophysics*, *35*, 245–296.

Iverson, R. M. (2000). Landslide triggering by rain infiltration. *Water Resources Research*, *36*, 1897–1910.

Izenman, A. J. (2013). Linear discriminant analysis. In *Modern multivariate statistical techniques*, *Springer Texts in Statistics* (pp. 237–280). New York, NY: Springer.

Jakob, M., & Hungr, O. (2005). *Debris-flow hazards and related phenomena* (p. 798). Chichester, UK: Springer.

Johnson, A. M., & Rodine, J. R. (1984). Debris flow. In D. Brunsden, & D. B. Prior (Eds.), *Slope instability* (pp. 257–361). Chichester, UK: John Wiley and Sons Ltd.

Kean, J. W., McCoy, S. W., Tucker, G. E., Staley, D. M., & Coe, J. A. (2013). Runoff-generated debris flows: Observations and modeling of surge initiation, magnitude, and frequency. *Journal of Geophysical Research: Earth Surface*, *118*, 2190–2207. https://doi.org/10.1002/jgrf.20148

Kirschbaum, D. B., Stanley, T., & Simmons, J. (2015). A dynamic landslide hazard assessment system for Central America and Hispaniola. *Natural Hazards and Earth System Sciences*, *15*, 2257–2272.

Koutsoyiannis, D., Kozonis, D., & Manetas, A. (1998). A mathematicalframework for studying rainfall intensity-duration-frequency relationships. *Journal of Hydrology*, *206*, 118–135.

Larsen, I. J., Pederson, J. L., & Schmidt, J. C. (2006). Geologic versus wildfire controls on hillslope processes and debris flow initiation in the Green River canyons of Dinosaur National Monument. *Geomorphology*, *81*, 114–127.

Linsley, R. K., Kohler, M. A., & Paulhus, J. L. H. (1982). *Hydrology for engineers* (3rd ed.). New York: McGraw-Hill.

Ma, C., Deng, J., & Wang, R. (2018). Analysis of the triggering conditions and erosion of a runoff-triggered debris flow in Miyun County, Beijing, China. *Landslides*, *15*, 2475–2485.

Melillo, M., Brunetti, M. T., Peruccaccim, S., Gariano, S. L., & Guzzetti, F. (2015). An algorithm for the objective reconstruction of rainfall events responsible for landslides. *Landslides*, *12*, 311–320.

Montgomery, D. R., Schmidt, K. M., Dietrich, W. E., & McKean, J. (2009). Instrumental record of debris flow initiation during natural rainfall: Implications for modelling slope stability. *Journal of Geophysical Research*, *114*, F01031. https://doi.org/10.1029/2008JF001078

Gabet, E. J., & Mudd, S. M. (2006). The mobilization of debris flows from shallow landslides. *Geomorphology*, *74*(1–4), 207–218.

Okano, K., Suwa, H., & Kanno, T. (2012). Characterization of debris flows by rainstorm condition at a torrent on the mount Yakedake volcano, Japan. *Geomorphology*, *136*(1), 88–94.

Osanai, N., Shimizu, T., Kuramoto, K., Kojima, S., & Noro, T. (2010). Japanese early-warning for debris flows and slope failures using rainfall indices with radial basis function network. *Landslides*, *7*, 325–338.

Pastorello, R., D'Agostino, V., & Hurlimann, M. (2020). Debris flow triggering characterization through a comparative analysis among different mountain catchments. *Catena*, *186*, 1–14.

Peres, D. J., & Cancelliere, A. (2014). Derivation and evaluation of landslide triggering thresholds by a Monte Carlo approach. *Hydrology and Earth System Sciences Discussions*, *11*, 2759–2794.

Philip, J. R. (1957). The theory of infiltration: Sorptivity and algebraic infiltration equation. *Soil Science*, *84*, 257–264.

Posner, A. J., & Georgakakos, K. P. (2015). Soil moisture and precipitation thresholds for real-time landslide prediction in El Salvador. *Landslides*, *12*(6), 1179–1196.

Postance, B., Hillier, J., Dijkstra, T., & Dixon, N. (2017). Comparing threshold definition techniques for rainfall-induced landslides: A national assessment using radar rainfall. *Earth Surface Processes and Landforms*, *43*(2), 553–560.

Prancevic, J. P., Lamb, M. P., & Fuller, B. M. (2014). Incipient sediment motion across the river to debris flow transition. *Geology*, *42*(3), 191–194.

Priestley, S. (2015). A conceptual model of the SCS runoff method. Stormwater conference, Water, New Zealand.

Rao, C. (1948). The utilization of multiple measurements in problems of biological classification. *Journal of the Royal Statistical Society: Series B: Methodological*, *10*(2), 159–203.

Saito, H., Nakayama, D., & Matsuyama, H. (2010). Relationship between the initiation of a shallow landslide and rainfall intensity— Duration thresholds in Japan. *Geomorphology*, *118*, 167–175.

Salciarini, D., Tamagnini, C., Conversini, P., & Rapinesi, S. (2012). Spatially distributed rainfall thresholds for the initiation of shallow landslides. *Natural Hazards*, *61*, 229–245.

Segoni, S., Piciullo, L., & Gariano, S. L. (2018). A review of the recent literature on rainfall thresholds for landslide occurrence. *Landslides*, *15*, 1483–1501.

Singh, V. P. (1996). *Kinematic wave modelling in water resources—Surface water hydrology*. John Wiley & Sons: US.

Soil Conservation Service (1972). *National engineering handbook, (NEH4)*. Washington, D. C: U.S. Dep. of Agric.

Staley, D. M., Kean, J. W., Cannon, S. H., Schmidt, K. M., & Laber, J. L. (2013). Objective definition of rainfall intensity-duration thresholds for the initiation of post-fire debris flows in southern California. *Landslides*, *10*, 547–562.

Staley, D. M., Negri, J. A., Kean, J., Laber, J. L., Libery, A. C., & Youberg, A. M. (2017). Prediction of spatially explicit rainfall intensity– duration thresholds for post-fire debris-flow generation in the western United States. *Landslides*, *10*, 547–562.

Takahashi, T. (1978). Mechanical characteristics of debris flow. *Journal of Hydraulics Division, ASCE*, *104*, 1153–1169.

Takahashi, T. (2019). *Debris Flow: Mechanics, prediction and countermeasures*. United Kingdom: Taylor & Francis Ltd.

Thomas, M. A., Mirus, B. B., & Collins, B. D. (2018). Identifying physics-based thresholds for rainfall-induced landsliding. *Geophysical Research Letters*, *45*, 9651–9661. https://doi.org/10.1029/2018GL079662

Tognacca, C., Bezzola, G. R., & Minor, H. E. (2000). Threshold criterion for debris flow initiation due to channel bed failure. In G. F. Wiezczorek, & N. D. Naeser (Eds.), *Proceedings of the Second International Conference on Debris Flow Hazards Mitigation Taipei, August* (pp. 89–97). Rotterdam: Balkema.

UKMO (2007). Fact sheet no. 3: Water in the atmosphere, Tech. rep., United Kingdom Meteorological Office.

Underwood, S. J., Schultz, M. D., Berti, M., Gregoretti, C., Simoni, A., Mote, T. L., & Saylor, A. M. (2016). Atmospheric circulation patterns, cloud-to-ground lightning, and locally intense convective rainfall associated with debris flow initiation in the Dolomite Alps of northeastern Italy. *Natural Hazards and Earth System Sciences*, *16*, 509–528.

Van Asch, T., Malet, J. P., Van Beek, L. P. H., & Amitrano, D. (2007). Techniques, advances, problems and issues in numerical modelling of landslide hazard. *Bulletin de la Societe Geologique de France*, *178*(2), 65–88.

Wilson, R. C., & Wiezoreck, G. F. (1995). Rainfall thresholds for the initiation of debris flows at La Honda, California. *Environmental and Engineering Geoscience*, *1*(1), 11–27.

Wu, Y., Lan, H., Gao, X., Li, L., & Yang, Z. (2015). A simplified physically based coupled rainfall threshold model for triggering landslides. *Engineering Geology*, *195*, 63–69.

Yu, B., Zhu, Y., Wang, T., Chen, Y., Zhu, Y., Tie, Y., & Lu, K. (2014). A prediction model for debris flows triggered by a runoff-induced mechanism. *Natural Hazards*, *74*, 1141–1116.

Zhou, W., & Tang, C. (2014). Rainfall thresholds for debris flow initiation in the Wenchuan earthquake-stricken area, southwestern China. *Landslides*, *11*(5), 877–887.